Analysis Report on

Iron and Lead Corrosion in WIPP-Relevant Conditions

Prepared by:
Luzheng Zhang, Priya Hora, Jay Jang, Leslie Kirkes, and Chammi Miller
Repository Performance Department (08882)

Task 4.4.2.2.1

Sandia National Laboratories
Carlsbad, NM 88220

WIPP:4.4.2.2.1:TD:QA-L:RECERT:546084

Information Only

APPROVAL PAGE

Author:	Luzheng Zhang, Org. 08882	9/22/2021 Date
Author:	***Signature on File*** Priya Hora, Org. 08882	09/22/2021 Date
Author:	***Signature on File*** Jay Jang, Org. 08882	09/22/2021 Date
Author:	***Signature on File*** Leslie Kirkes, Org. 08882	09/22/2021 Date
Author:	Chammi Miller, Org. 08882	09/22/2021 Date
Technical Reviewer:	***Signature on File*** David Enos, Org. 01852	09/22/2021 Date
QA Reviewer:	Shelly Nielsen, Org. 08880	9-22-2021 Date
Management Reviewer:	Antonio Triventi, Org. 08882	9/22/2021 Date

Information Only

TABLE OF CONTENTS

LIST OF FIGURES 5
LIST OF TABLES 8
ABBREVIATIONS, ACRONYMS AND INITIALISMS 9
1. INTRODUCTION 13
2. MATERIALS, ANALYSES AND CHARACTERIZATION 14
2.1. Materials 14
2.1.1. Coupons 14
2.1.2. Brine solutions 14
2.2. Chemical Analysis and Characterization of Samples 15
3. SINGLE-PASS FLOW THROUGH METHOD 16
3.1. Method and Corrosion Rates 16
3.1.1. Experimental setup 16
3.1.2. Corrosion rate by metal release to solution 16
3.1.3. Corrosion rate by mass loss 17
3.1.4. Corrosion rate by surface retreat under interferometry 18
3.2. Results by SPFT and Discussion 19
3.2.1. SPFT experiments and operation conditions 19
3.2.2. Fe release concentration 20
3.2.3. Mass loss in SPFT 27
3.2.4. Surface retraction by interferometry 30
3.2.5. Characterization of corrosion products 32
4. STATIC REACTION METHOD 37
4.1. Method and Corrosion Rates 37
4.1.1. Experimental setup 37
4.1.2. Corrosion rate by H_2 generation 37
4.2. Results by Static Method and Discussion 38
5. ELECTROCHEMICAL METHOD 39
5.1. Method and Corrosion Rates 39
5.1.1. Experimental setup 39
5.1.2. Corrosion rate by electrochemical tests 39
5.1.3. Data Analysis of Electrochemical Measurements 41
5.2. Results by EIS/PDP Tests and Discussion 41
5.2.1. EIS and PDP tests 41

Information Only

5.2.2. Corrosion rates 44
6. SUMMARY 49
7. ACKNOWLEDGEMENTS 50
8. REFERENCES 51
APPENDIX A 53
APPENDIX B 65

Information Only

LIST OF FIGURES

Figure 1. Plot of mass loss measurements after each cleaning cycle. Line segment AB represents the loss of corrosion products and pristine metal. BC represents loss of pristine steel. BC is extrapolated backwards to point D which is the final projected mass of the coupon..... 17

Figure 2. An illustration of interferometry technique. A mask (RTV sealant) is applied to the surface of a steel coupon and placed into a reactor. Solution reacts with the exposed surface of steel, causing dissolution and surface retreat. The mask is then removed revealing the pristine surface. This change in height can then be measured with interferometry. 18

Figure 3. Fe concentrations (ppb) in the effluent of each reactor from the 6-month SPFT experiments at 90 °C: (a) Overall Fe concentration profiles, (b) a zoom-in view..... 21

Figure 4. pHr Changes of the effluent in each reactor from the 6-month SPFT experiments at 90 °C. 22

Figure 5. A comparison of Fe concentrations (orange lines) to pHr values (blue lines) of the effluent in each reactor from the 6-month SPFT experiments with different brine solutions at 90 °C: (a) 1.0 m NaCl, (b) 3.5 m NaCl, (c) 0.32 m $MgCl_2$, (d) 0.90 m $MgCl_2$, (e) GWB, and (f) ERDA-6. 23

Figure 6. Fe concentration vs. ionic strength of the starting brine solutions from the 6-month SPFT experiments at 90 °C at different time frames (from 1 to 6 months)..... 24

Figure 7. Fe corrosion rates calculated from Fe concentrations in the 6-month SPFT experiments in different brine solutions at 90 °C: (a) Overall Corrosion rate profiles, (b) a Zoom-in view of corrosion rates in brines 1.0 m NaCl, GWB and ERDA-6. Error bars represent 10% uncertainty from ICP-MS. 26

Figure 8. Average corrosion rates determined by Fe release concentrations in different brines from 6-month SPFT experiments at 90 °C. Error bars represent one standard deviation.. 27

Figure 9. Mass loss of Fe coupon in each reactor from SPFT experiments at 90 °C for 6 months: (a) 1.0 m NaCl, (b) 3.5 m NaCl, (c) 0.32 m $MgCl_2$, (d) 0.90 m $MgCl_2$, (e) GWB, and (f) ERDA-6. 29

Figure 10. Corrosion rates determined by mass loss of Fe coupons in different brines from 6-month SPFT experiments at 90 °C. A negative corrosion rate (-0.7 μm/year) was obtained for GWB because -15.6 mg mass was gained..... 30

Figure 11. Interferometry analyses of (a) polished C1018 coupon surface and (b) the polished surface after a RTV silicone drop were removed (AB: RTV protected and then removed surface; BC: polished and no RTV protected surface). Note: PV plots in (a) and (b) have different scales at the Y-Axis. 31

Figure 12. Average corrosion rates determined by interferometry on the C1018 cleaned coupon surfaces removed from 6-month SPFT experiments with different brine solutions at 90 °C. 34

Figure 13. Average corrosion rates of C1018 by Fe release, mass loss and interferometry from the 6-month SPFT experiments with different brine solutions at 90 °C. 34

Information Only

Figure 14. SEM Images of the Fe coupon surface from the 6-month SPFT experiment in GWB at 90 °C. 35

Figure 15. SEM Image and EDS analysis of the Fe coupon surface removed from the 6-month SPFT experiment in GWB at 90 °C and EDS analyses of solid particles on the surface. 36

Figure 16. (a) A typical EIS spectra and phase angles from electrochemical cell test, (b) Tafel extrapolation from a potentiodynamic polarization test. 40

Figure 17. EIS spectra and phase angles of C1018 coupons in the SGWB brine with N_2 bubbling in solution at 90 °C. 42

Figure 18. EIS spectra and phase angles of C1018 coupons in the SGWB brine with N_2 in headspace at 90 °C. 43

Figure 19. PDP data of C1018 coupon in the SGWB brine with (a) N_2 bubbling in solution, (b) N_2 filling in headspace at 90 °C. 44

Figure 20. Corrosion rates of C1018 coupon vs. time in SGWB at 90 °C with (a) N_2 bubbling in solution, (b) N_2 filling in headspace. Error bars represent the standard deviations determined by triplicate measurements. 48

Figure A-1. Photos of Fe coupon surface in 1.0 m NaCl from a 6-month SPFT experiment at 90 °C: (a) termination with masks, (b) termination with masks removed, and (c) after surface cleaning. 53

Figure A-2. Photos of Fe coupon surface in 3.5 m NaCl from a 6-month SPFT experiment at 90 °C: (a) termination with masks, (b) termination with masks removed, and (c) after surface cleaning. 54

Figure A-3. Photos of Fe coupon surface in 0.32 m $MgCl_2$ from a 6-month SPFT experiment at 90 °C: (a) termination with masks, (b) termination with masks removed, and (c) after surface cleaning. 55

Figure A-4. Photos of Fe coupon surface in 0.90 m $MgCl_2$ from a 6-month SPFT experiment at 90 °C: (a) termination with masks, (b) termination with masks removed, and (c) after surface cleaning. 56

Figure A-5. Photos of Fe coupon surface in GWB from a 6-month SPFT experiment at 90 °C: (a) termination with masks, (b) termination with masks removed, and (c) after surface cleaning. 57

Figure A-6. Photos of the Fe coupon surface in ERDA-6 from a 6-month SPFT experiment at 90 °C: (a) termination with masks, (b) termination with masks removed, and (c) after surface cleaning. 58

Figure A-7. Interferometry analysis of the Fe coupon surface in 1.0 m NaCl from the 6-month SPFT experiment at 90 °C. 59

Figure A-8. Interferometry analysis of the Fe coupon surface in 3.5 m NaCl from the 6-month SPFT experiment at 90 °C. 60

Figure A-9. Interferometry analysis of the Fe coupon surface in 0.32 m $MgCl_2$ from the 6-month SPFT experiment at 90 °C. 61

Information Only

Figure A-10. Interferometry analysis of the Fe coupon surface in 0.90 m $MgCl_2$ from the 6-month SPFT experiment at 90 °C. 62

Figure A-11. Interferometry analysis of the Fe coupon surface in GWB from the 6-month SPFT experiment at 90 °C. 63

Figure A-12. Interferometry analysis of the Fe coupon surface in ERDA-6 from the 6-month SPFT experiment at 90 °C. 64

Information Only

LIST OF TABLES

Table 1. Chemical composition of the C1018 steel coupons used in SPFT [a] 14

Table 2. A list of brine solutions used in Fe corrosion tests and their compositions (a) or recipes (b)..... 15

Table 3. A summary of 6 SPFT experiments and operation conditions 19

Table 4. Fe corrosion rates (μm/year) calculated from Fe concentrations in the effluent of each reactor from 6-month SPFT experiments with different brine solutions at 90 °C..... 25

Table 5. Mass loss and corrosion rate of Fe coupons in each reactor from 6-month SPFT experiments at 90 °C [a] 28

Table 6. Surface changes (μm) in height of C1018 coupon surfaces removed from the 6-month SPFT experiments with different brine solutions at 90 °C..... 33

Table 7. A summary of corrosion rates (μm/year) of C1018 by different analysis techniques from the 6-month SPFT experiments with different brine solutions at 90 °C 33

Table 8. A summary of electrochemical experiments for the C1018 coupons in the SGWB solution at 90 °C 41

Table 9. A summary of polarization resistances (Ohm), R_p, estimated by EIS measurements for the C1018 coupons in the SGWB solution at 90 °C..... 45

Table 10. A summary of Tafel slopes β_a and β_c (V/decade) and the Stern-Geary coefficient B estimated by PDP measurements for the C1018 coupons in the SGWB solution at 90 °C..... 45

Table 11. A summary of corrosion rates (μm/year) by the electrochemical method for the C1018 coupons in the SGWB solution at 90 °C 47

Table B-1. Fe concentrations (ppb) in the effluent of each reactor from 6-month SPFT experiments at 90 °C [a] 65

Table B-2. pHr values of the starting brine solutions and the effluent of each reactor from 6-month SPFT experiments at 90 °C 66

Information Only

ABBREVIATIONS, ACRONYMS AND INITIALISMS

Abbreviation or Acronym	Definition
2x	double
10X	10 times
50X	50 times
%	percent
A	exposure surface area
Am	americium
AR	Analysis Report
AP	Analysis Plan
ASTM	American Society for Testing and Materials
atm	Atmosphere, unit of pressure
Ave.	Average
β_a	the Tafel slope of anodic reaction
β_c	the Tafel slope of cathodic reaction
B	the Stern-Geary coefficient
C	concentration of ions or coulomb (unit of electric charge)
°C	temperature in Celsius
$CaCl_2$	calcium chloride
CE	Counter Electrode
CFR	Code of Federal Regulations
cm	centimeter
CO_2	carbon dioxide
CPE	Constant Phase Elements
CRA	Compliance Recertification Application
Δh	change in height measured with interferometry
ΔP	change in pressure
Δt	change in time
DAS	Data Acquisition System
DO	Dissolved Oxygen

Information Only

DOE	Department of Energy
DI	deionized
e	electron
E	electrical potential
E_{corr}	electrical potential of corrosion
Eoc	open circuit potential
EDS	Energy Dispersive Spectroscopy
EIS	Electrochemical Impedance Spectroscopy
EPA	Environmental Protection Agency
ERDA-6	Energy Research and Development Administration well 6
ES&H	Environment, Safety and Health
F	Faraday constant
Fe	iron
$Fe(OH)_2(s)$	solid iron (II) hydroxide
FY	Fiscal Year
F_w	Formula weight
GC	Gas Chromatography
GWB	Generic Weep Brine
H_2	hydrogen gas
H_2O	water
Hz	Hertz, unit of frequency
I	current
i_{corr}	corrosion current density
IC	Ion Chromatography
ICP-MS	Inductively Coupled Plasma Mass Spectrometry
ID	Inner Diameter
IR	Infrared
ISO	International Organization for Standardization
K	Kelvin, unit of temperature
KCl	potassium chloride
kg	kilogram

Information Only

L	Liter
LiCl	lithium chloride
m	molality, mol/kg H_2O
M&TE	Measuring and Test Equipment
mm	millimeter
MΩ	Megaohm
mg	milligram
$MgCl_2$	magnesium chloride
mL	milliliter
n	mole of electrons for an anodic or cathodic reaction
N_2	nitrogen gas
NaCl	sodium chloride
$Na_2B_4O_7 \cdot 10H_2O$	sodium tetraborate decahydrate
NaBr	sodium bromide
Na_2SO_4	sodium sulfate
NIST	National Institute of Standards and Technology
NP	Nuclear (Waste Management) Procedure
O_2	oxygen
PA	Performance Assessment
Pb	lead
PDP	Potentiodynamic Polarization
pH	negative logarithm of hydrogen ion activity
pHr	pH reading
PTFE	polytetrafluoroethylene
Pu	plutonium
PV	Peak-Valley
QA	Quality Assurance
r	corrosion rate
ρ	density of tested material
R	universal gas constant
RE	Reference Electrode

Information Only

R_p	polarization resistance
RT	Room Temperature
RTV	Room Temperature Vulcanized
SCE	Saturated Calomel Electrode
SEM	Scanning Electron Microscope
SGWB	Simple Generic Weep Brine
SNL	Sandia National Laboratories
SP	(Activity/Project) Specific Procedure
SPFT	Single-Pass Flow Through
Std. Dev.	Standard Deviation
t	time exposure to corrosion condition
T	absolute temperature
TEM	Transmission Electron Microscopy
Th	thorium
TP	Test Plan
TRU	transuranic
U	uranium
UHP	Ultrahigh Purity
µA	micro-ampere
UV-Vis	Ultraviolet-Visible
V	Volt or flow rate of brine to reactor
W	Weight (mass) loss
WE	Working Electrode
WIPP	Waste Isolation Pilot Plant
wt.	weight
XRD	X-ray Diffractometer

Information Only

1. INTRODUCTION

The Waste Isolation Pilot Plan (WIPP) is a repository for transuranic (TRU) waste, located within the bedded salts of the Permian Salado Formation, southern New Mexico. This formation consists of an interbedded halite-and-anhydrite formation overlaying the Castile Formation. The WIPP performance assessment (PA) calculations demonstrate compliance of the repository (U.S. (U.S. EPA, 1996a, 1996b), including the consequences of future inadvertent human drilling intrusions into the repository; such intrusions could lead to a postulated release of radionuclides (e.g., U, Pu, Th, Am, etc.) to the accessible environment before the end of the 10,000-year regulatory period. The U.S. Department of Energy (DOE) has examined different drilling scenarios, which involve the penetration of the repository by one or more drill holes; some of the scenarios also involve the possibility of the penetration of a pressurized Castile brine reservoir (U.S. DOE, 2004). The estimated quantity of radionuclides released to the accessible environment following penetration of the repository depends on the chemistry of these radioactive elements.

The nature of the environment within the WIPP following closure will, to a large extent, control the speciation of the radionuclides within the waste. Components contained within the waste, such as the metals undergoing active corrosion, can impact the oxidative or reductive nature of the repository environment. Active corrosion within the WIPP will serve to maintain electrochemically reducing conditions. The predominant metals within the WIPP are iron (Fe) and lead (Pb), present within the waste itself, as well as the containers used to hold the emplaced waste.

Relatively large quantities of metallic iron will be present in the repository in the form of steel waste containers and as iron-based alloys in the waste. Over 63,000 metric tons of iron-based materials waste and packaging materials in contact-handed (CH) and remote-handled (CH) waste are estimated to be present in the repository at closure (Van Soest, 2018). Trapped oxygen in the repository upon closure will be quickly consumed, establishing an anoxic environment. Based on these established parameters, it is assumed that all corrosion will occur under anoxic conditions (U.S. DOE, 2019).

Corrosion is the oxidation of a metal by electrochemical reactions controlled by repository conditions such as brine composition, gas composition, temperature, and pressure. Iron corrosion has been identified as one of major gas generation processes in the WIPP (Brush, 1995). Lead corrosion was not considered in gas generation due to lower inventory compared to iron, however, it may become a contributor with a recently increased lead inventory (Kirkes, 2019). To measure iron/lead corrosion rates at WIPP-relevant conditions, the test plan (TP) TP 06-02 Rev. 3 (Sisk-Scott and Icenhower, 2016) has summarized details of corrosion reactions and corrosion tests, including experimental methods, tasks, data quality control, chemical analysis, and chemical characterization techniques.

A recent milestone report (Zhang, 2020) has summarized iron corrosion experiments in 6 different brines solutions (without sulfide) at 90 °C using various experimental methods including Single-Pass Flow Through (SPFT), static, and the electrochemical measurements. The scope of this analysis report (AR) is to present data analysis of experimental data documented in the FY20 milestone report (Zhang, 2020). These corrosion rates will be used in WIPP PA calculations to estimate the gas generation by corrosion reactions.

Information Only

2. MATERIALS, ANALYSES AND CHARACTERIZATION

2.1. Materials

2.1.1. Coupons

The material C1018 steel from Alabama Specialty Products Inc. was used in all experiments. The dimensions of those coupons used in SPFT and electrochemical experiments are different. The coupon surfaces (all sides) for SPFT experiments were polished by the Sandia National Laboratories (SNL) Metallurgy and Materials Joining Department (Org. 01831), while the button coupons (diameter=0.5") for static experiments were cleaned with isopropanol only before placing into a reactor. The coupon (disc-like, diameter=1") surface (one side) used in electrochemical tests was polished and cleaned (see Appendix A in the milestone report by Zhang (2020)), then examined by interferometer for the surface roughness. It was shown that the surface roughness is 0.03 μm for the mirror-like coupons used in SPFT experiments and it is 0.3 μm for the coupons used in electrochemical tests. The composition of the steel, provided by the vendor, is listed in **Table 1**.

Table 1. Chemical composition of the C1018 steel coupons used in SPFT [a]

Element	C	Mn	P	S	Si	Cu	Ni	Cr	Mo	Fe
Concentration, wt.%	0.184	0.75	0.011	0.014	0.017	0.10	0.08	0.10	0.023	98.72

[a] This composition is provided by the vendor Alabama Specialty Products, as determined by ASTM-A108. The concentrations are directly from the vendor's report.

2.1.2. Brine solutions

All brine solutions were prepared from reagent grade chemicals from Fisher Scientific or analogous vendors, and DI water was provided by ELGA Purelab Flex 2 system with a resistivity of 18.2 MΩ·cm.

Table 2 lists all brine solutions and their compositions or recipes. Brine solutions used in SPFT experiments were prepared by dissolving desired mass of salts (NaCl, $MgCl_2 \cdot 6H_2O$, etc.) in DI water. Prior to preparing a brine solution, the DI water was degassed inside a glovebox for at least 2 hours, using an electric air pump to equilibrate with internal gas of the glovebox (oxygen level less than 5 ppm). The brine solutions GWB and ERDA-6 were prepared by mixing the desired salts in 1.0 kg DI water according to the recipes described in WIPP Activity/Project Specific Procedure (SP) SP 20-4, *Preparing Synthetic Brines for Geochemical Experiments.*

For brine solutions used in electrochemical tests, the desired salts (NaCl, $MgCl_2 \cdot 6H_2O$, or both) were dissolved in the DI water and the resulting solution was then degassed in a fume hood (outside glovebox) for 2 hours, using a stream of UHP N_2 gas.

Information Only

Table 2. A list of brine solutions used in Fe corrosion tests and their compositions (a) or recipes (b)

Brine Name	**(a) Composition** (m = mol/kg-water)
1.0 m NaCl	1.00 m
3.5 m NaCl	3.50 m
0.32 m $MgCl_2$	0.32 m
0.90 m $MgCl_2$	0.90 m
SGWB	3.20 m NaCl + 0.90 m $MgCl_2$
GWB	See recipe below *
ERDA-6	See recipe below *

(b) Recipe of GWB and ERAD-6

Chemical Formula	**GWB**	**ERDA-6**
	Grams in 1.0 kg DI water	
NaCl	202.32	293.38
$MgCl_2 \cdot 6H_2O$	233.23	4.33
KCl	39.25	8.11
Na_2SO_4	28.42	26.58
$Na_2B_4O_7 \cdot 10H_2O$	16.96	6.73
$CaCl_2 \cdot 2H_2O$	2.29	1.97
NaBr	3.09	1.27
LiCl	0.21	none

* The recipes of GWB and ERAD-6 are from SP 20-4, *Preparing Synthetic Brines for Geochemical Experiments*.

2.2. Chemical Analysis and Characterization of Samples

For all procedures listed in this AR, the most current revision of such documents was used for data analysis.

The pH of all liquid samples (unfiltered) was determined using a Ross Sure-flow pH electrode and a pH meter as per SP 12-14, *Use of pH Meters and Electrodes*. This pH value is the reading (denoted as pHr) of the Ross pH probe. Elemental concentrations of interest are determined using the Perkin Elmer NexIon 300D inductively coupled plasma mass spectrometer (ICP-MS) as per SP 12-31, *Calibration, Use and Maintenance of the Perkin Elmer NexIon 300D ICP-MS*.

Corrosion products were collected and characterized using Bruker D8 X-ray diffractometer (XRD) according to SP 12-8, *Use and Maintenance of Bruker Analytical X-Ray Systems D8 Advance X-Ray Diffractometer* and JEOL JSM 5900LV scanning electron microscope (SEM) equipped with a Thermo NORAN System 7 energy dispersive X-ray spectrometer (EDS) according to SP 12-17, *Scanning Electron Microscope Imaging and Energy Dispersive Spectroscopy*.

Information Only

3. SINGLE-PASS FLOW THROUGH METHOD

3.1. Method and Corrosion Rates

3.1.1. Experimental setup

The SPFT experimental setup is designed to simulate realistic conditions if brine penetration into the WIPP repository. A full description of the experimental setup and methodology can be found in the FY20 milestone report (Zhang, 2020).

The SPFT corrosion experiments with steel coupons (C1018) were run in 6 different brines (1.0 m NaCl, 3.5 m NaCl, 0.32 m $MgCl_2$, 0.90 m $MgCl_2$, GWB and ERDA-6) at 90 °C for approximatively 6 months. Other brines such as SGWB will be also included in the future SPFT experiments. The steel coupons were then removed from each reactor for cleaning and characterization. Corrosion products, if present, were collected for characterization by XRD and/or SEM/EDS. Liquid from the reactor effluent was sampled throughout the duration of the test for chemical analyses (pH and Fe release concentration). Corrosion rates were determined from the measured Fe release rate. As discussed later in Section 3.1.4, each steel coupon had a series of regions that were coated with RTV silicone to protect 5 specific regions. The surface area of these regions was subtracted from the actual coupon surface area for determining corrosion rates described in sections 3.1.2 and 3.1.3.

3.1.2. Corrosion rate by metal release to solution

Effluent samples were collected weekly to measure the Fe release rate into solution during the test. The dissolution rate of Fe at time j can be determined from the following equation:

$$r_j = \frac{VC_{j,out}}{\rho A} \times 0.00365 \quad (1)$$

where

r_j – Corrosion rate at time j , μm/year

V – Flow rate of brine to the reactor, mL/day

$C_{j,out}$ – Concentration of Fe in the effluent at time j, μg/L

A – Exposed surface area of the coupon, cm^2

ρ – Density of tested material, g/cm^3 (7.87 g/cm^3 for C1018)

Equation (1) is used to estimate the corrosion rate from the metal (Fe) concentration in the liquid phase only. The ICP-MS system has minimum detection limit of 5 ppm based upon calibration data, and a minimum resolvable corrosion rate of 0.024 μm/year given the surface area of the coupons evaluated in this study. If Fe-bearing solid corrosion product(s) are formed within the solution as a precipitate or on the steel surface without being observed by experimenters, the corrosion rate calculated by Equation (1) would be an underestimation. The corrosion rate of Fe determined by dissolved Fe concentration in the SPFT experiments needs to be corroborated by other measurement techniques (e.g., mass loss, interferometry) applied to the same coupons from the experiments.

Information Only

3.1.3. Corrosion rate by mass loss

The mass loss technique can compensate for the possible underestimation of corrosion rates calculated by Equation (1), because it measures the total mass change of each coupon relative to its initial mass, and is insensitive to whether corrosion products form on the surface, precipitate in the solution, or if the metal ions remain completely in solution.

The steel C1018 coupons were removed from the reactors and stored in the glovebox when the SPFT experiments were terminated. Following the ASTM standard G1-03 (ASTM, 2003), the corroded steel coupons were placed in a cleaning solution for approximately 5 minutes, removed, scrubbed gently, rinsed with DI water then ethanol and weighed. This process is repeated and then the final weight of the coupon (point D in **Figure 1**) is calculated graphically using a method outlined in ISO 8407 (ISO, 1991) and discussed by (Roselle, 2009). An example of this process is shown in **Figure 1**.

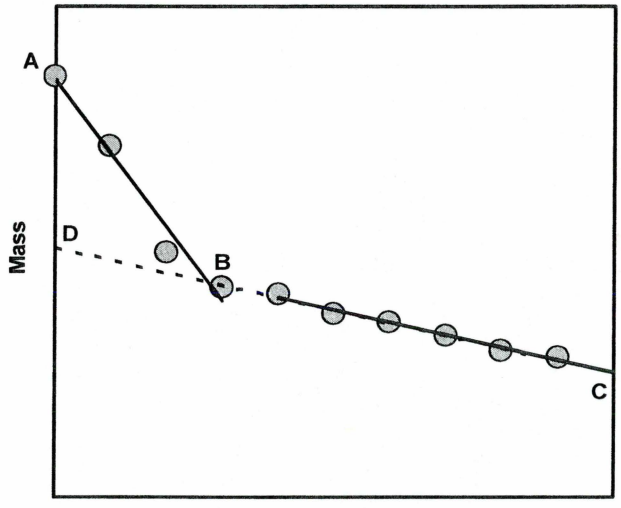

Figure 1. Plot of mass loss measurements after each cleaning cycle. Line segment AB represents the loss of corrosion products and pristine metal. BC represents loss of pristine steel. BC is extrapolated backwards to point D which is the final projected mass of the coupon.

The mass loss is calculated as the difference between the initial weight of coupon minus the final projected mass (point D in **Figure 1**). The corrosion rate in μm/year can be calculated using the following equation:

$$r = \frac{W \times 87.6}{A \times t \times \rho} \times 1000 \qquad (2)$$

where

r – Corrosion rate, μm/year

W – mass loss, mg

A – Exposed surface area of the coupon, cm^2

t – Time exposure to corrosion condition, hours

ρ – Density of tested materials, g/cm^3 ($7.87\ g/cm^3$ for C1018)

Information Only

The balance used to perform weight loss measurements has an accuracy of 0.1 mg which, given the surface area of the samples used in this study coupled with the length of the test, yields a minimum detectable corrosion rate of 0.004 μm/year.

It should be noted that this calculated rate is an average corrosion rate over the period of experimental time, not an instantaneous measure of corrosion rate (Roselle, 2011).

3.1.4. Corrosion rate by surface retreat under interferometry

The interferometer is a type of microscope that uses white light (with a green filter) and Mirau objectives (a 10X and 50X) to analyze the small displacements, refractive index changes and surface irregularities of a solid object. For the purposes of our experiments, the focus was the change of the steel coupon surface morphology. A detailed description of using the interferometer is present in SP 12-34, *Imaging using the vertical scanning interferometer*.

After 6 months of reaction, the SPFT coupons were cleaned according to the ASTM standard G1-03 (ASTM, 2003). The RTV silicon spots, implemented as a control, were removed to reveal the pristine unreacted surface. The cleaned coupon samples were then placed under the interferometer light in order to measure the direct surface retreat, illustrated in **Figure 2**. The dissolution rate can be calculated using the following equation:

$$r = \frac{\Delta h}{t} \tag{3}$$

where

r – Corrosion rate, μm/year

Δh – Change in height, μm

t – Time exposure to corrosion condition, years

The corrosion rate given by Equation (3) also represents an average corrosion rate over the period of experimental time, not an instantaneous measure of corrosion rate. The minimum resolvable surface retraction measurable via interferometry as implemented here is 0.01 μm, corresponding to a minimum resolvable corrosion rate of 0.02 μm/year.

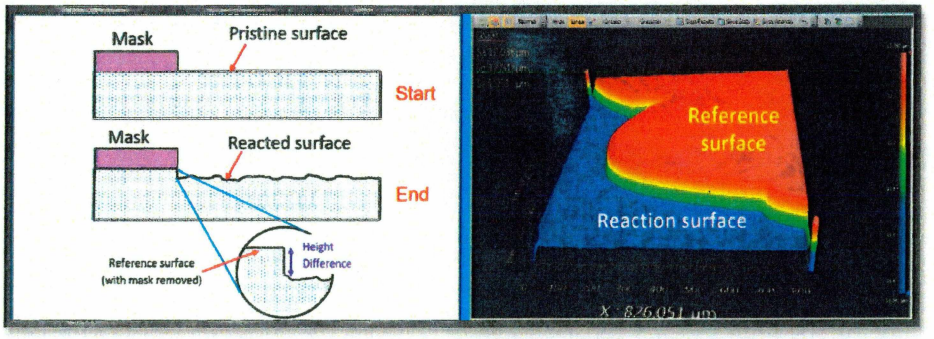

Figure 2. An illustration of interferometry technique. A mask (RTV sealant) is applied to the surface of a steel coupon and placed into a reactor. Solution reacts with the exposed surface of steel, causing dissolution and surface retreat. The mask is then removed revealing the pristine surface. This change in height can then be measured with interferometry.

Information Only

3.2. Results by SPFT and Discussion

3.2.1. SPFT experiments and operation conditions

A total of 6 SPFT experiments were completed in parallel within the same glovebox. **Table 3** summarizes all 6 SPFT experiments, reaction conditions, brine chemistry, and steel coupon dimensions. The exposed surface area represents the total surface area without the surface area of the 5 RTV silicone marks discussed in Section 3.1.1 (average: 2.2 cm^2).

Table 3. A summary of 6 SPFT experiments and operation conditions

Reactor #	**1**	**2**	**3**	**4**	**5**	**6**
Brine Solution						
Brine Name	3.5 m NaCl	1.0 m NaCl	0.32 m $MgCl_2$	0.90 m $MgCl_2$	ERDA-6	GWB
pHr [a]	8.6 ± 0.4	8.6 ± 0.3	7.9 ± 0.2	7.4 ± 0.3	8.3 ± 0.1	7.4 ± 0.2
Ionic strength, m	3.5	1.0	0.96	2.7	5.9	8.3
Flow rate, mL/day	60.0	60.0	60.0	60.0	60.0	60.0
Coupon #	**1**	**2**	**3**	**4**	**5**	**6**
Mass, g	115.6439	116.9599	114.8084	113.5232	122.0150	122.3581
Length, mm	49.31	48.39	48.07	47.80	50.61	50.59
Width, mm	50.58	50.64	50.62	50.53	51.15	51.04
Thickness, mm	6.08	6.05	6.02	6.05	6.02	6.05
Exposed surface area, cm^2	59.83	58.79	58.35	58.00	61.83	61.74
Operation Conditions						
Temperature, °C [b]	90	90	90	90	90	90
Test time, days	183	183	183	183	183	183

[a] An average of the pHr taken each time when a replacement brine solution was prepared for the duration of the experiment.

[b] Experiments were performed at the target temperature 90 ± 1°C.

The SPFT experiments in 6 brine solutions were run for about 6 months, then terminated. The coupons were retrieved in each reactor. The photos of each coupons are presented in **Figure** A-1 **to Figure A-6** (see Appendix A).

It should be noted that the data from SPFT experiments presented in this report represent a single set of samples, and that as such the overall experimental uncertainty cannot be quantified. Replicates have been planned and set up for future experiments under the same testing conditions. The data of replicated experiments will be reported in subsequent reports.

Information Only

3.2.2. Fe release concentration

For SPFT experiments, over 6-months effluents were sampled weekly to measure Fe concentrations using ICP-MS and pH readings (pHr) using of the brine. Ross pH probe. All Fe release concentrations and pHr values are summarized in **Table B-1** and **Table B-2**, respectively (see Appendix B).

Figure 3 plots iron (Fe) concentrations in ppb measured from the effluents. Generally, the dissolved concentration of Fe was scattered throughout the experiments. Higher Fe release was observed in $MgCl_2$ solutions than that in other brines (about 1-2 orders of magnitude). The Fe release was noticeably suppressed in GWB, which contains $MgCl_2$ concentration comparable to 0.90 m. One speculation of the scatter could be intermittent partial dislodging of the passivation layer from the surface, re-exposing the fresh Fe surface to the solution. The corrosion reaction was very slow under anoxic conditions, and the resulting corrosion product layer was thin and compact on the metal surface – the voluminous corrosion product layer anticipated for steel under oxic conditions was not present.

pHr (pH reading) is one of the main factors impacted by the corrosion rate. **Figure 4** shows the pHr changes over the time of the SPFT experiments. The pHr was also plotted individually for each brine coupled with the iron release over time (**Figure 5**). The pHr values are confined within a range of 7.5 - 9.0, except for GWB.

Figure 6 presents the relationship between the Fe concentration and the ionic strength at each month during the SPFT experiments. Among all 6 brines, the Fe concentration in solution was the highest in the 0.90 m $MgCl_2$ brine (I = 2.7 m) at all times. The brines with higher ionic strengths (>3.5 m) show lower Fe concentrations, indicating slower Fe corrosion rates. This information might be useful for evaluating the effect of brine concentration on the corrosion rate.

From the Fe concentration released into brines, the Fe corrosion rates can be calculated by Equation (1), as listed in **Table 4**. **Figure 7a** presents a profile of Fe corrosion rates calculated from Fe concentrations in the 6-month SPFT experiments with different brine solutions at 90 °C. The highest corrosion rates were observed in 0.90 m $MgCl_2$. The order of corrosion rate change in different brine solutions was: 0.90 m $MgCl_2$ > 0.32 m $MgCl_2$ > 3.5 m NaCl > (1.0 m NaCl ~ GWB ~ ERDA-6). The corrosion rates in the three brine solutions (1.0 m NaCl, GWB, and ERDA-6) do not show a significant difference, as shown in **Figure 7b**. The observation of higher initial rates for both of these brines, which fell off to a very low rate with time could have resulted from salt film formation on the surface, in effect coating the material and hindering further dissolution.

Figure 8 shows an average of Fe corrosion rates over the 6-month SPFT experiments listed in **Table 4**. The average corrosion rates were estimated from Fe release over the period of experimental time (6 months). A standard deviation was obtained by each of the averages and used as error bars in **Figure 8**. It shows that the Fe coupon in 0.9 m $MgCl_2$ brine has the highest corrosion rate (4.3 ± 2.5 μm/year) than in any other brines. Rates determined for 3.5 m NaCl, GWB, ERDA-6 in one set of SPFT show large standard deviations. Data from another set of SPFT experiments are in collection/analysis and will be documented/analyzed in another milestone report and AR.

Information Only

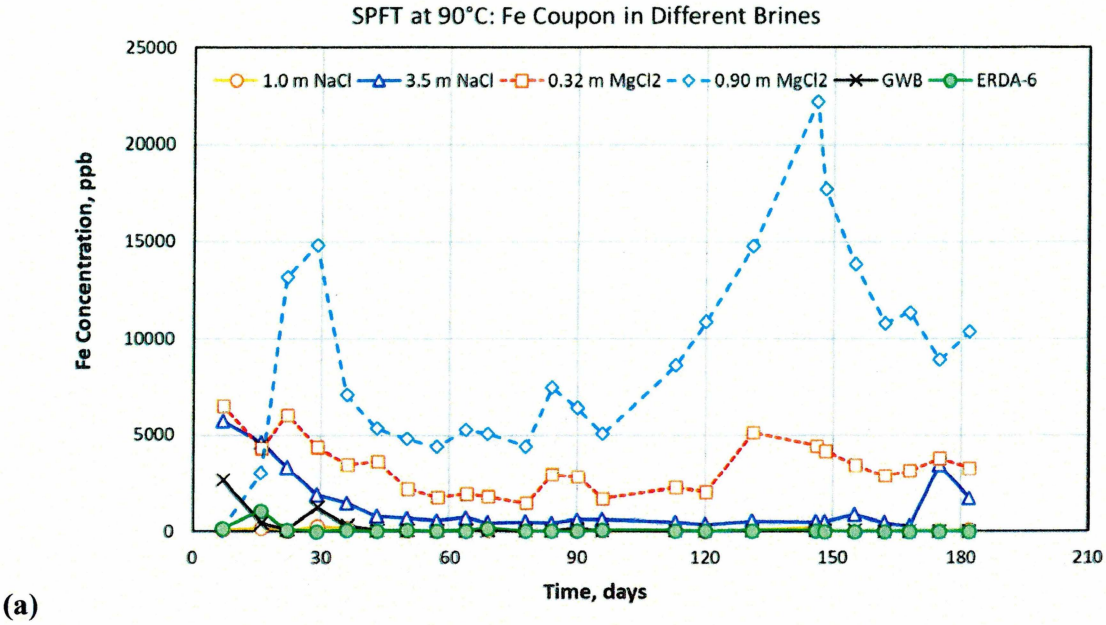

(a)

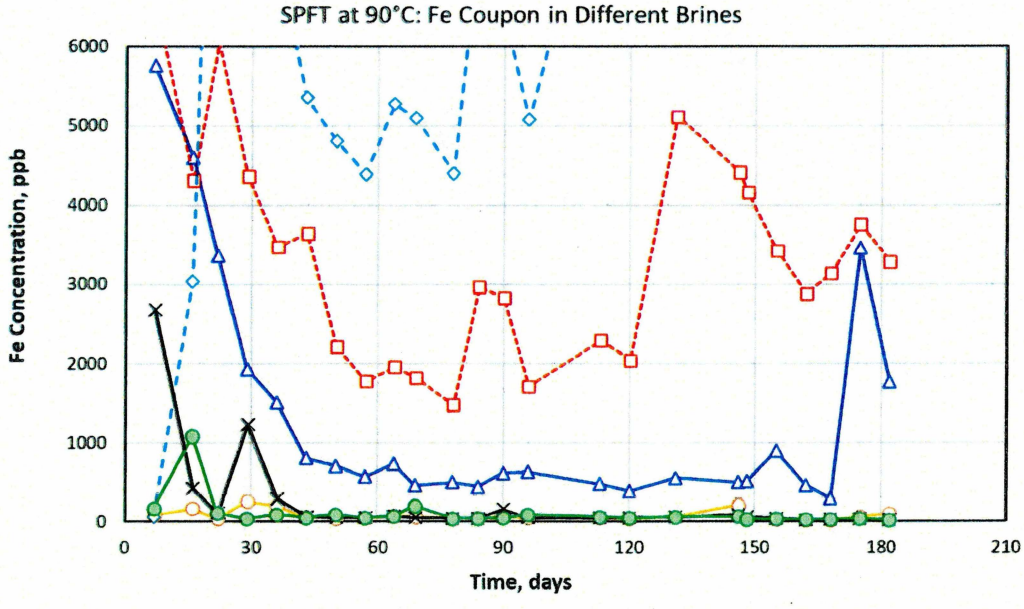

(b)

Figure 3. Fe concentrations (ppb) in the effluent of each reactor from the 6-month SPFT experiments at 90 °C: (a) Overall Fe concentration profiles, (b) a zoom-in view.

Information Only

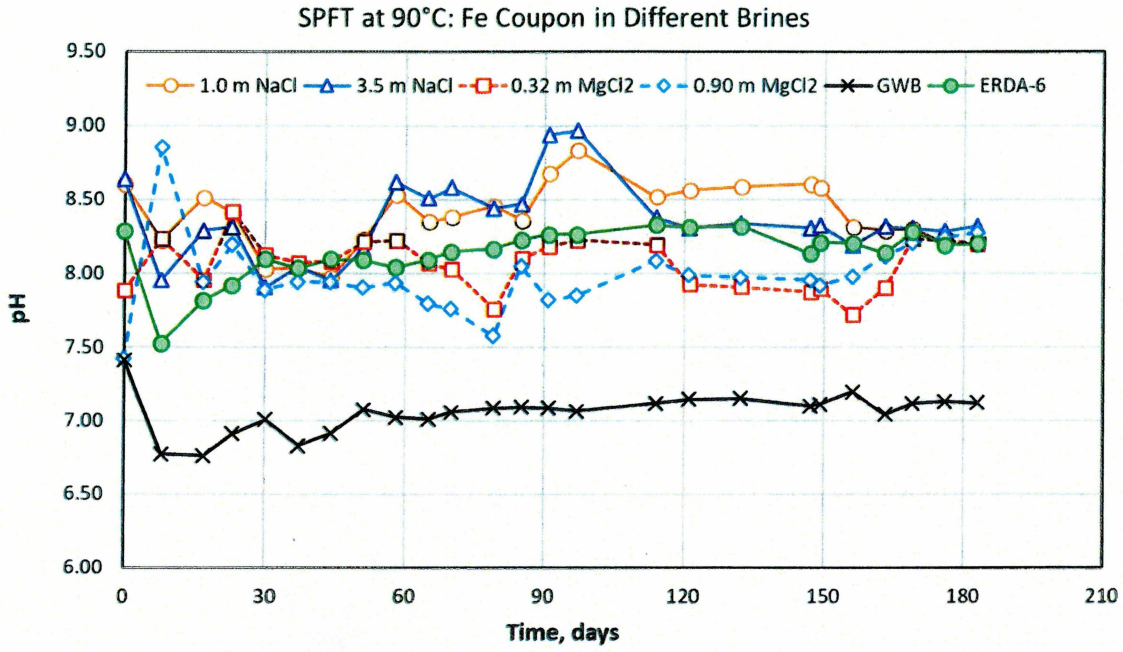

Figure 4. pHr Changes of the effluent in each reactor from the 6-month SPFT experiments at 90 °C.

Information Only

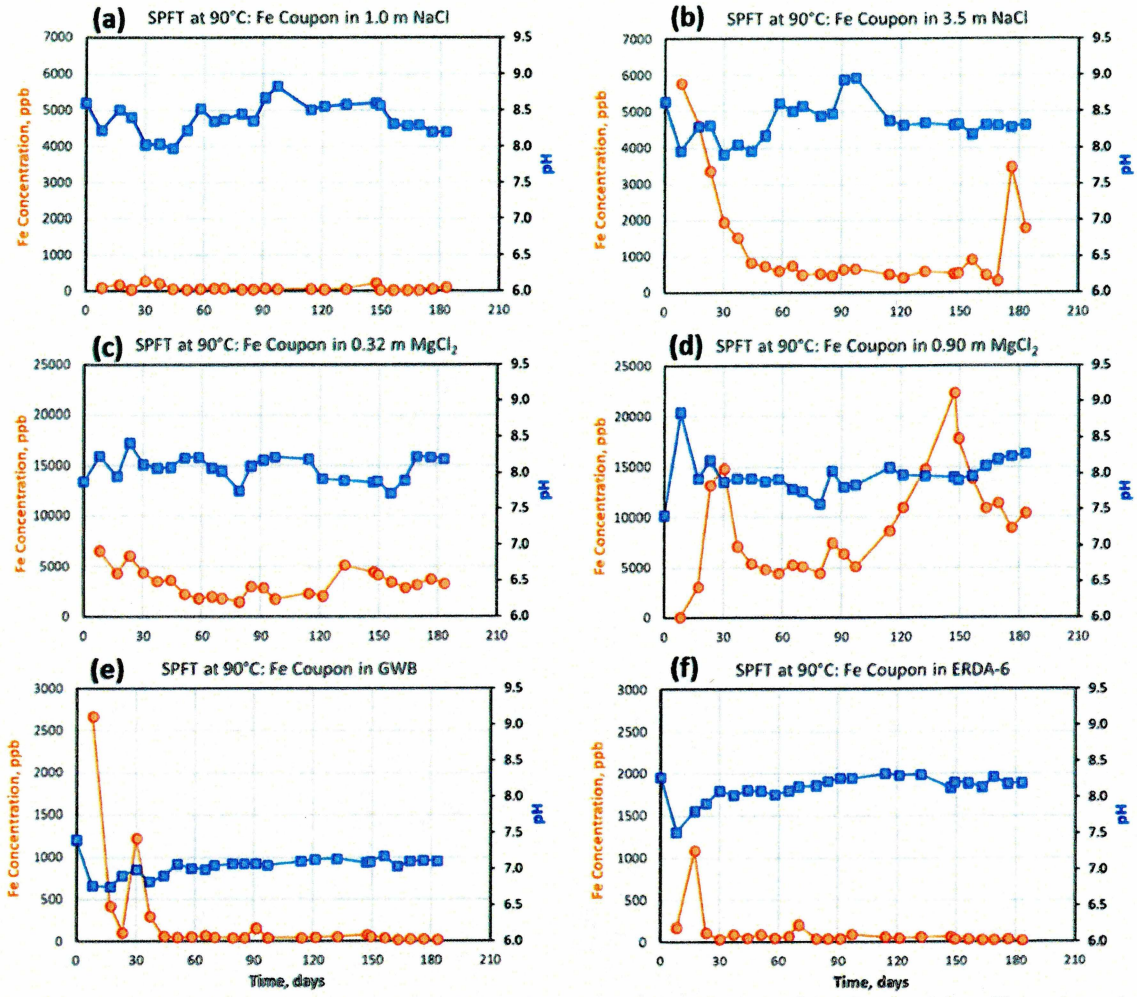

Figure 5. A comparison of Fe concentrations (orange lines) to pHr values (blue lines) of the effluent in each reactor from the 6-month SPFT experiments with different brine solutions at 90 °C: (a) 1.0 m NaCl, (b) 3.5 m NaCl, (c) 0.32 m $MgCl_2$, (d) 0.90 m $MgCl_2$, (e) GWB, and (f) ERDA-6.

Information Only

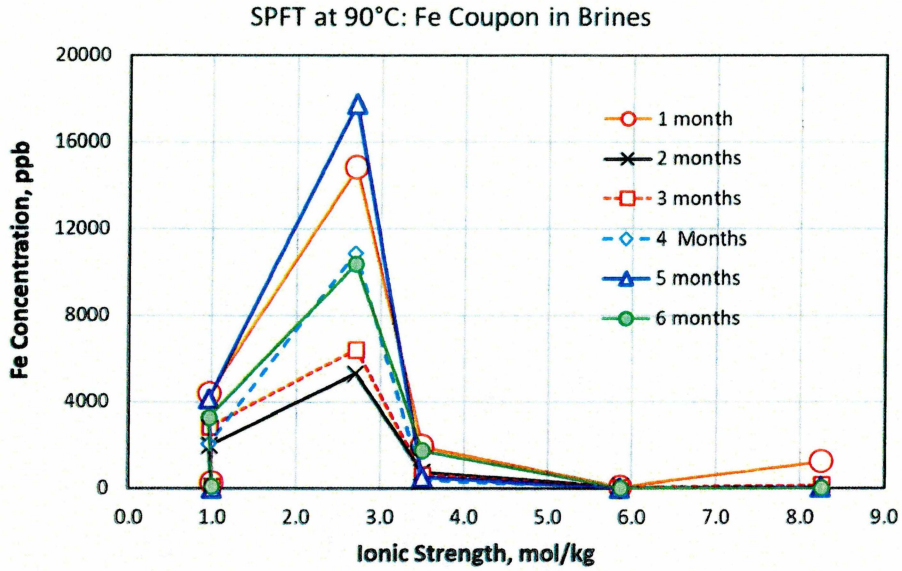

Figure 6. Fe concentration vs. ionic strength of the starting brine solutions from the 6-month SPFT experiments at 90 °C at different time frames (from 1 to 6 months).

Information Only

Table 4. Fe corrosion rates (μm/year) calculated from Fe concentrations in the effluent of each reactor from 6-month SPFT experiments with different brine solutions at 90 °C.

Time, days	Week #	1.0 m NaCl	3.5 m NaCl	0.32 m $MgCl_2$	0.90 m $MgCl_2$	GWB	ERDA-6
8	1	0.04	2.73	3.11	0.03	1.20	0.08
17	2	0.08	2.18	2.06	1.46	0.19	0.49
23	3	0.02	1.59	2.88	6.32	0.05	0.05
30	4	0.12	0.92	2.08	7.10	0.55	0.02
37	5	0.10	0.72	1.66	3.40	0.14	0.04
44	6	0.03	0.38	1.74	2.57	0.03	0.02
51	7	0.02	0.34	1.06	2.31	0.02	0.04
58	8	0.02	0.27	0.85	2.11	0.03	0.02
65	9	0.04	0.35	0.94	2.53	0.03	0.03
70	10	0.03	0.22	0.87	2.45	0.02	0.09
79	11	0.02	0.24	0.70	2.11	0.02	0.02
85	12	0.02	0.21	1.41	3.58	0.02	0.02
91	13	0.03	0.30	1.35	3.07	0.07	0.02
97	14	0.02	0.30	0.82	2.44	0.02	0.04
114	15	0.02	0.23	1.09	4.13	0.02	0.03
121	16	0.02	0.19	0.98	5.22	0.02	0.02
132	17	0.03	0.27	2.44	7.08	0.03	0.03
147	18	0.10	0.24	2.10	10.67	0.04	0.03
149	19	0.02	0.24	1.98	8.51	0.03	0.02
156	20	0.01	0.43	1.63	6.64	0.02	0.02
163	21	0.01	0.22	1.37	5.19	0.01	0.01
169	22	0.01	0.14	1.50	5.46	0.01	0.01
176	23	0.03	1.64	1.79	4.27	0.01	0.02
183	24	0.05	0.84	1.57	4.98	0.01	0.01
Average		0.04	0.63	1.58	4.32	0.11	0.05
Std. Dev.		0.03	0.70	0.65	2.49	0.26	0.10

Information Only

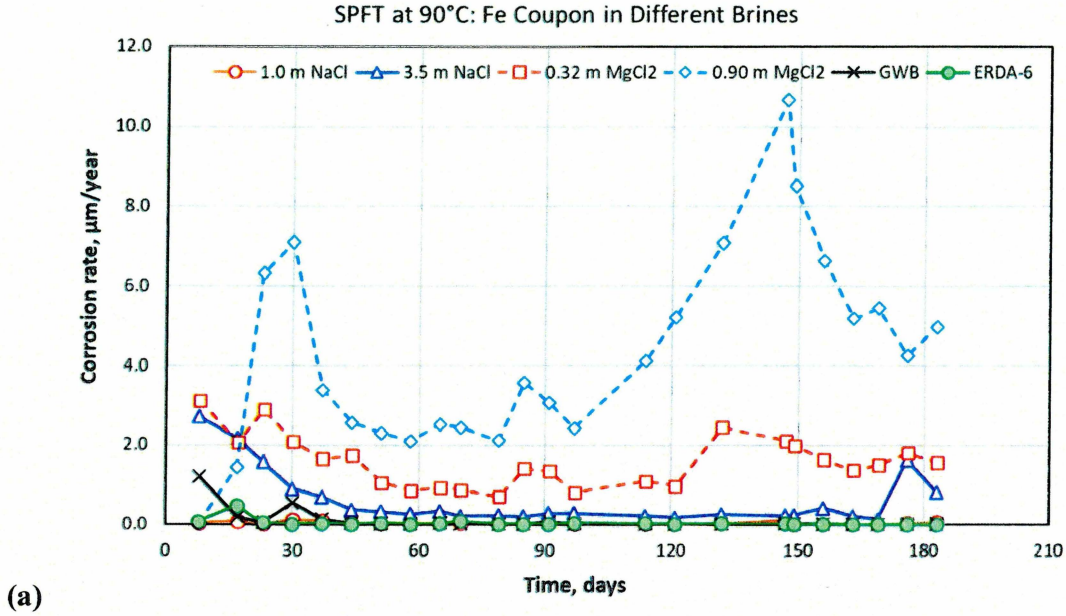

(a)

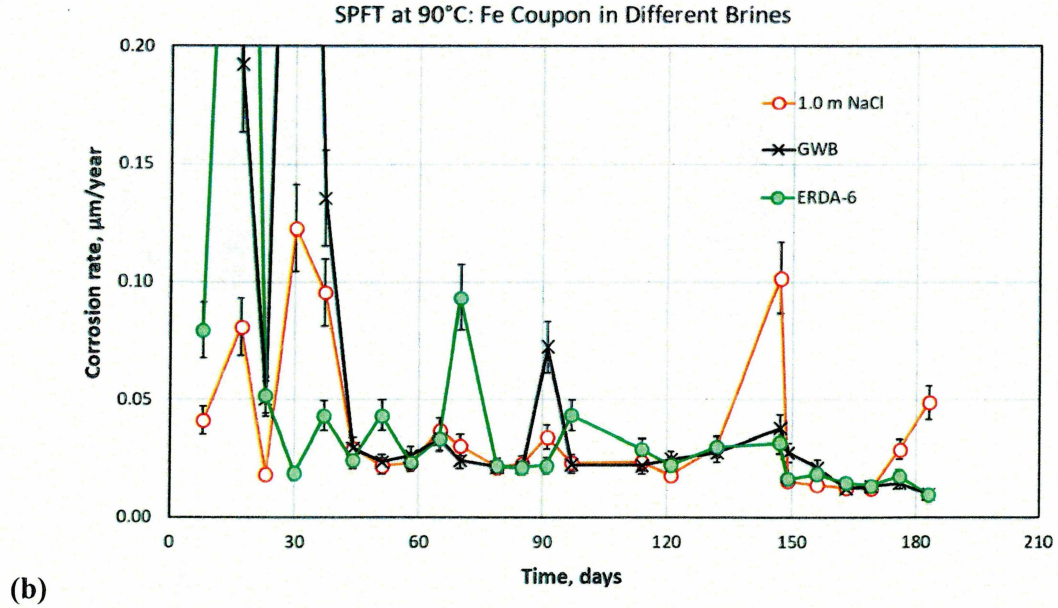

(b)

Figure 7. Fe corrosion rates calculated from Fe concentrations in the 6-month SPFT experiments in different brine solutions at 90 °C: (a) Overall Corrosion rate profiles, (b) a Zoom-in view of corrosion rates in brines 1.0 m NaCl, GWB and ERDA-6. Error bars represent 10% uncertainty from ICP-MS.

Information Only

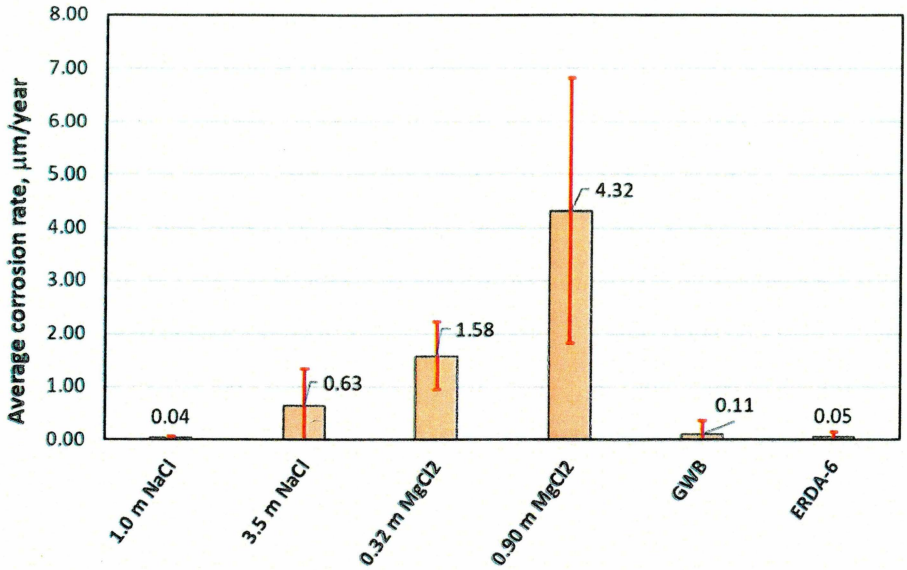

Figure 8. Average corrosion rates determined by Fe release concentrations in different brines from 6-month SPFT experiments at 90 °C. Error bars represent one standard deviation.

3.2.3. Mass loss in SPFT

When the SPFT experiments were terminated, all Fe coupons were removed from each reactor and then cleaned to estimate corrosion rates by the mass loss technique.

Figure A-1 to Figure A-6 (see Appendix A) show the images of the Fe coupons at termination with masks, at termination with masks removed, and after cleaning from brine solutions 1.0 m NaCl, 3.5 m NaCl, 0.32 $MgCl_2$, 0.90 m $MgCl_2$, GWB, and ERDA-6, respectively. Because of the high concentration of salts in GWB and ERDA-6, some white deposits were observed on the steel C1018 coupon surface before cleaning (**Figure A-5** and **Figure A-6**), but identified to be non-corrosion products. All white deposits on these two surfaces were able to clean; therefore, these deposits could be salt residues. The deposited layer may hinder further reaction, resulting in a low corrosion rate. However, there is no hard evidence to show the impact of salt deposition on corrosion rate. The initial weight and mass of Fe coupons after each cleaning cycle were summarized in **Table 5**. The mass loss of each coupon also listed in **Table 5**.The mass data are also plotted as mass vs. cycle in **Figure 9**. It should be noted that there were more solids deposited on the coupon in GWB solution and more cleaning cycles were performed. However, 15.6 mg (as shown in **Table 5**) was gained in the final weight after 12 cleaning cycles, resulting in a negative corrosion rate of - 0.7 µm/year for the coupon in GWB. **Figure 10** presents Fe corrosion rates determined by mass loss in different brines except GWB.

The trend of corrosion rates determined by mass loss generally agrees with those by the chemical analysis of Fe release (**Figure 8**) and by surface retract analysis under interferometer (see Section 3.2.4) for all brine solutions, except GWB. The coupon corroded in GWB gained 15.6 mg, resulting in a negative corrosion rate (-0.7 µm/year). It could be due to the descaling of solid (salt precipitation) in the cleaning process (SEM/EDS images presented in Section 3.2.5). The negative corrosion rate in less corrosive brine (GWB) could be due to an artifact of mass loss technique. It should be cautioned to use the corrosion rate determined by the mass loss technique, particularly, when the corrosion rate is very low (< 1 µm/year). Regardless, the corrosion rates in brine solutions

Information Only

(3.5 m NaCl, 0.32 m $MgCl_2$, 0.90 m $MgCl_2$, and ERDA-6) are comparable to those determined by Fe release and by interferometry techniques (**Table 7**).

Table 5. Mass loss and corrosion rate of Fe coupons in each reactor from 6-month SPFT experiments at 90 °C [a]

Coupon # / Brine	1 3.5 m NaCl	2 1.0 m NaCl	3 0.32 m $MgCl_2$	4 0.9 m $MgCl_2$	5 ERDA-6	6 GWB
Mass after cleaning cycle #, g						
Cleaning cycle 1	115.6365	116.9373	114.7380	113.4130	122.0069	123.3333
Cleaning cycle 2	115.6366	116.9282	114.7343	113.4083	122.0024	123.0053
Cleaning cycle 3	115.6341	116.9270	114.7318	113.4064	122.0026	122.8313
Cleaning cycle 4	115.6320	116.9267	114.7312	113.4062	122.0010	122.6849
Cleaning cycle 5	115.6322	116.9265	114.7310	113.4058	122.0006	122.5400
Cleaning cycle 6	115.6320	116.9264	114.7307	113.4056	122.0008	122.4013
Cleaning cycle 7						122.3510
Cleaning cycle 8						122.3290
Cleaning cycle 9						122.3229
Cleaning cycle 10						122.3220
Cleaning cycle 11						122.3218
Cleaning cycle 12						122.3219
Starting Weight, g	115.6439	116.9599	114.8084	113.5232	122.015	122.3581
Final Weight [b], g	115.6321	116.9276	114.7328	113.4073	122.0039	122.3737
mass loss, mg	11.8	32.3	75.6	115.9	11.1	-15.6
Corrosion rate [c], µm/year	0.5	1.4	3.3	5.1	0.5	-0.7

[a] The fourth decimal place of weight measurements on balance is subject to uncertainty.

[b] Final weights are determined by extrapolating the mass loss over cleaning cycles as shown in **Figure 9**.

[c] The corrosion rates were calculated by Eq (2) and coupon information listed in **Table 3**.

Information Only

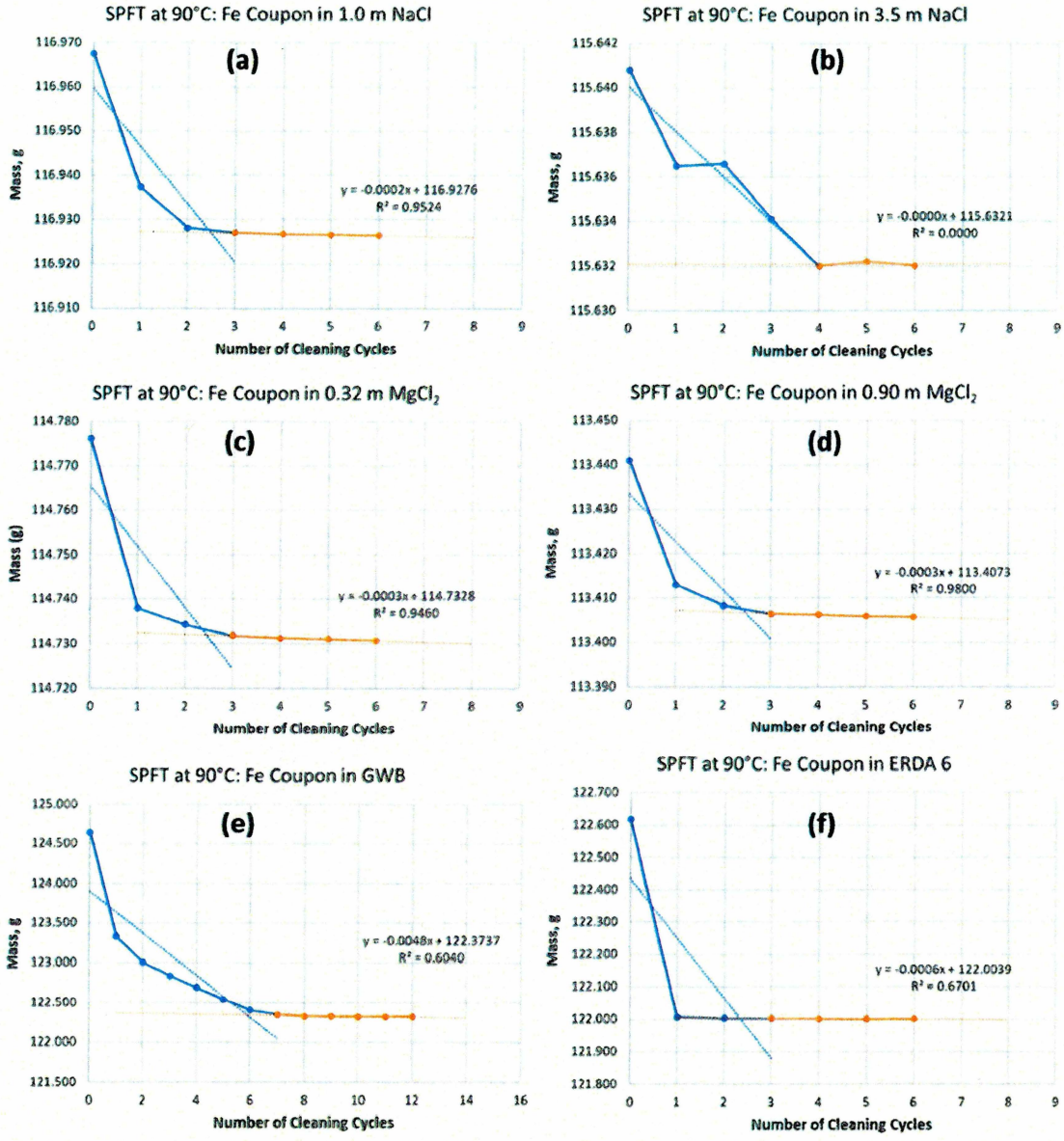

Figure 9. Mass loss of Fe coupon in each reactor from SPFT experiments at 90 °C for 6 months: (a) 1.0 m NaCl, (b) 3.5 m NaCl, (c) 0.32 m $MgCl_2$, (d) 0.90 m $MgCl_2$, (e) GWB, and (f) ERDA-6.

Information Only

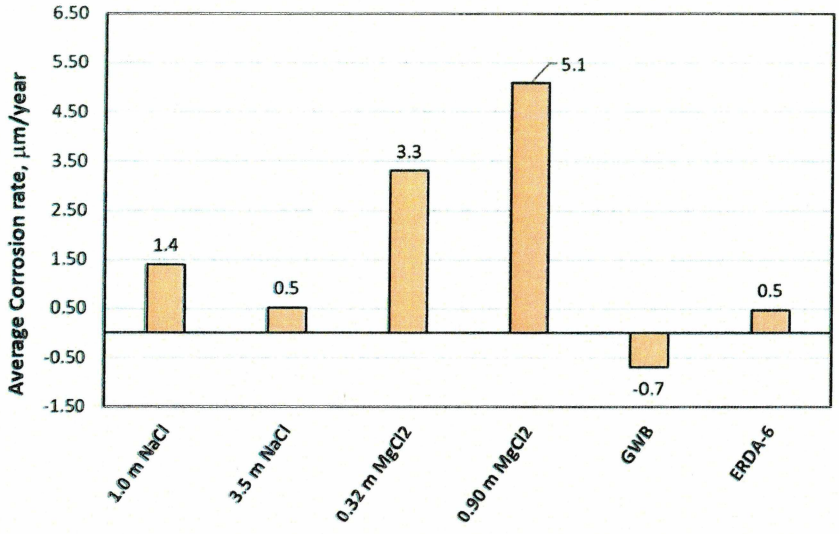

Figure 10. Corrosion rates determined by mass loss of Fe coupons in different brines from 6-month SPFT experiments at 90 °C. A negative corrosion rate (-0.7 µm/year for GWB) indicates mass gain.

3.2.4. Surface retraction by interferometry

The cleaned coupon surfaces were also analyzed using the interferometer to determine the surface change in height. To validation testing on the spot(s) covered by RTV silicone, a fresh coupon with removed RTV silicone drops was examined. As shown in **Figure 11(a)**, the polished surface (stored in glovebox and transferred outside for immediate analysis by the interferometer at the ambient condition in the air) is relatively flat where the peak to valley (PV) is about 0.03 µm. When a protective RTV drop was removed after drying in the air, it was found that (1) there was no residual material left behind (region AB in **Figure 11(b)**), (2) the PV in the region covered by a RTV silicon drop (AB) was the same as the one in the region uncovered (on the right end of BC). The uncovered surfaces have some retracted spots (on the left end of BC in **Figure 11(b)**), indicating some corrosion occurred on the polished and uncovered surfaces while the coupon was exposed to the air for drying and analysis, while the surface covered was protected by the RTV drop (region AB **Figure 11(b)**). Therefore, the RTV silicon can be used as corrosion protection layer in the SPFT experiments and the RTV-covered surface can be used as a reference for surface retraction analysis by the interferometry.

Figure A-7 to **Figure A-12** in Appendix A show the interferometry images of the C1018 coupon cleaned surface and their PV profiles from brine solutions 1.0 m NaCl, 3.5 m NaCl, 0.32 $MgCl_2$, 0.90 m $MgCl_2$, GWB, and ERDA-6, respectively. Obviously, the surface exposed to a brine solution shows deep valleys (give the depth values here), indicating that the coupon surfaces were corroded, while the protected surface (masked by silicone drops) shows no sign of any corrosion. The protected surface is the reference to measuring the surface change in height under interferometry.

Information Only

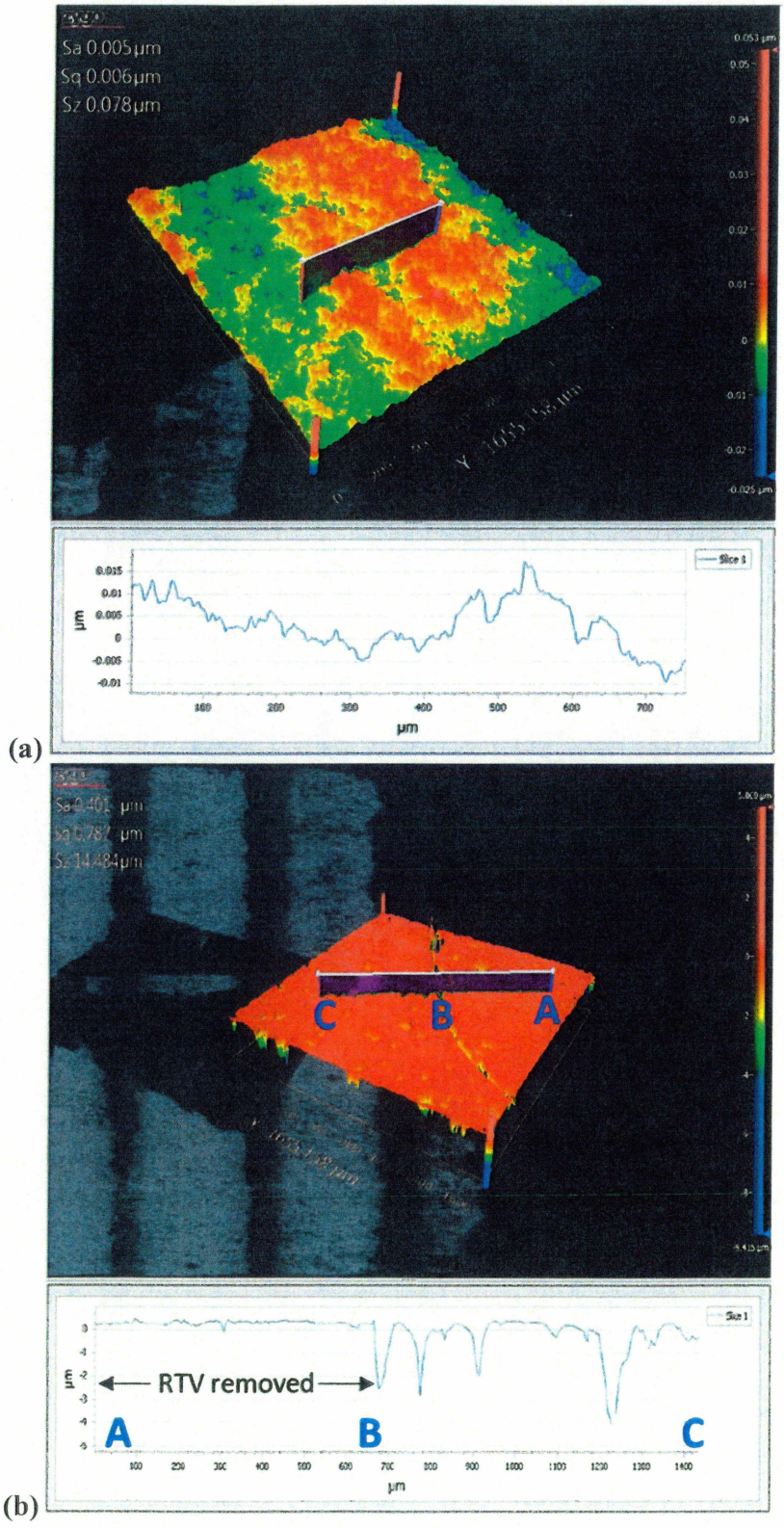

Figure 11. Interferometry analyses of (a) polished C1018 coupon surface and (b) the polished surface after a RTV silicone drop were removed (AB: RTV protected and then removed surface; BC: polished and no RTV protected surface). Note: PV plots in (a) and (b) have different scales at the Y-Axis.

Information Only

For each coupon, five locations were selected for measuring the surface retreat, and an average was used to calculate the final corrosion rate. The most reacted steel coupons were found in the 0.9 m $MgCl_2$ brine, while the steel coupon surfaces slightly changed height in the NaCl, GWB, and ERDA-6 brines. These observations on the interferometry images generally agree with those from Fe released concentrations shown in **Figure 3**. From the average change in height, the corrosion rate of Fe coupon can be calculated by Equation (3). **Figure 12** presents the average corrosion rates (2x surface changes in height listed in **Table 6**) of the C1018 coupons in all 6 brines by interferometry (the error bars shown in this figure were obtained by averaging the retreated surface at 5 different spots). Generally, they agree with the Fe release (**Figure 3**) and the mass loss (**Table 5**).

Table 7 summarizes corrosion rates of C1018 from the same SPFT experiments with three analysis techniques: Fe release, mass loss, and interferometry (see also in **Figure 13**). Standard deviations presented in **Table 7** were obtained from corrosion rates over the period of test time (6 months), except for the mass loss technique where one corrosion rate value for each brine was determined at the termination time of SPFT experiments. It is shown that the corrosion rates in the same brine solution are slightly different by these three methods, particularly in the brine with less corrosion (e.g., GWB). On the other hand, the corrosion rates in brines with higher corrosion (0.32 m and 0.90 m $MgCl_2$) shows the smaller difference by three techniques. In addition, the corrosion rates estimated by the interferometry seem to have a lower value than the other two techniques. Generally, the trend of the corrosion rate vs. brine solution looks similar among the three techniques. The order is 0.90 m $MgCl_2$ > 0.32 m $MgCl_2$ > 3.5 m NaCl > (1.0 m NaCl ~ ERDA-6 ~ GWB). It should be noted that the results for each combination of brine chemistry and measurement technique are for a single sample, and as such, do not capture sample to sample variability. For better statistic results, more SPFT experiments have been performed and data will be reported/analyzed in the future reports.

3.2.5. Characterization of corrosion products

Before cleaning the coupons removed from the SPFT experiments, there weren't visible solid particles on all surfaces, except for the one in GWB (Reactor #6), where there was a lot of salt deposition (see **Figure A-5**). No solid was recovered at the bottom of the reactors. While cleaning the coupons from the SPFT experiments, there were not enough solid-like corrosion products to be collected for XRD characterization.

Some particles (solid-like islands) were found on the cleaned coupon surfaces from Reactor #6, containing the GWB brine. **Figure 14** and **Figure 15** show SEM/EDS analysis, respectively. The EDS analysis shows the oxidation of iron resulting from corrosion reactions on the coupon surface. However, the SEM/EDS analysis on the cleaned surface may not directly be used to identify the "corrosion products' of the C1018 coupon in SPFT experiments.

The solid-like particles may be the evidence that some mass was gained for the coupon in GWB brine (see **Table 5**).

Information Only

Table 6. Surface changes (μm) in height of C1018 coupon surfaces removed from the 6-month SPFT experiments with different brine solutions at 90 °C

Location #	1.0 m NaCl	3.5 m NaCl	0.32 m $MgCl_2$	0.90 m $MgCl_2$	GWB	ERDA-6
1	-0.26	-0.23	-1.33	-1.58	-0.07	-0.84
2	-0.32	0.02	-1.33	-1.63	-0.24	-0.38
3	-0.49	-0.32	-1.02	-1.83	-0.48	-0.75
4	-0.70	-0.01	-1.21	-1.65	0.10	-0.18
5	-0.08	0.04	-1.18	-1.28	0.31	0.04
Ave.	-0.37	-0.10	-1.21	-1.59	-0.08	-0.42
Std. Dev.	0.23	0.16	0.13	0.20	0.30	0.37

Table 7. A summary of corrosion rates (μm/year) of C1018 by different analysis techniques from the 6-month SPFT experiments with different brine solutions at 90 °C

Brine Name	Fe Release		Mass loss		Interferometry	
	Ave.	Std. Dev.	Ave.	Std. Dev.	Ave.	Std. Dev.
1.0 m NaCl	0.04	0.03	1.40	-	0.74	0.23
3.5 m NaCl	0.63	0.70	0.52	-	0.20	0.16
0.32 m $MgCl_2$	1.58	0.65	3.30	-	2.43	0.13
0.90 m $MgCl_2$	4.32	2.49	5.08	-	3.19	0.20
GWB	0.11	0.26	-0.70	-	0.16	0.30
ERDA-6	0.05	0.10	0.48	-	0.84	0.37

Information Only

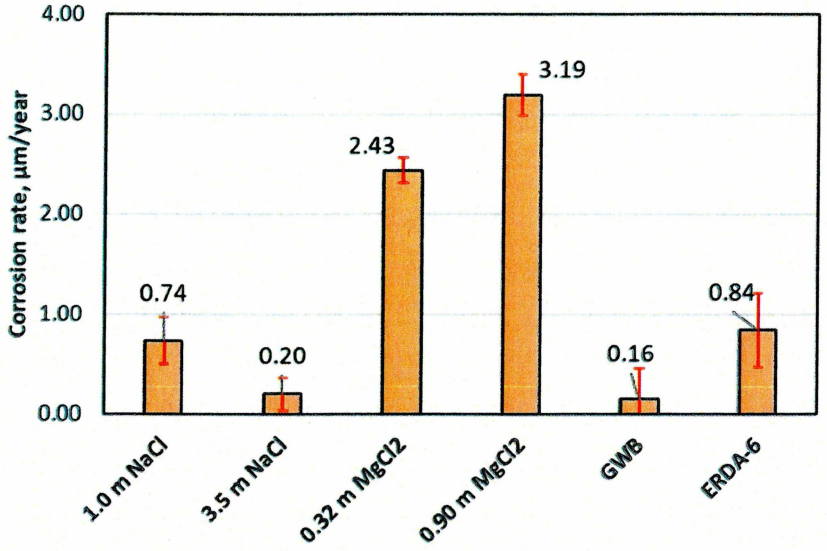

Figure 12. Average corrosion rates determined by interferometry on the C1018 cleaned coupon surfaces removed from 6-month SPFT experiments with different brine solutions at 90 °C.

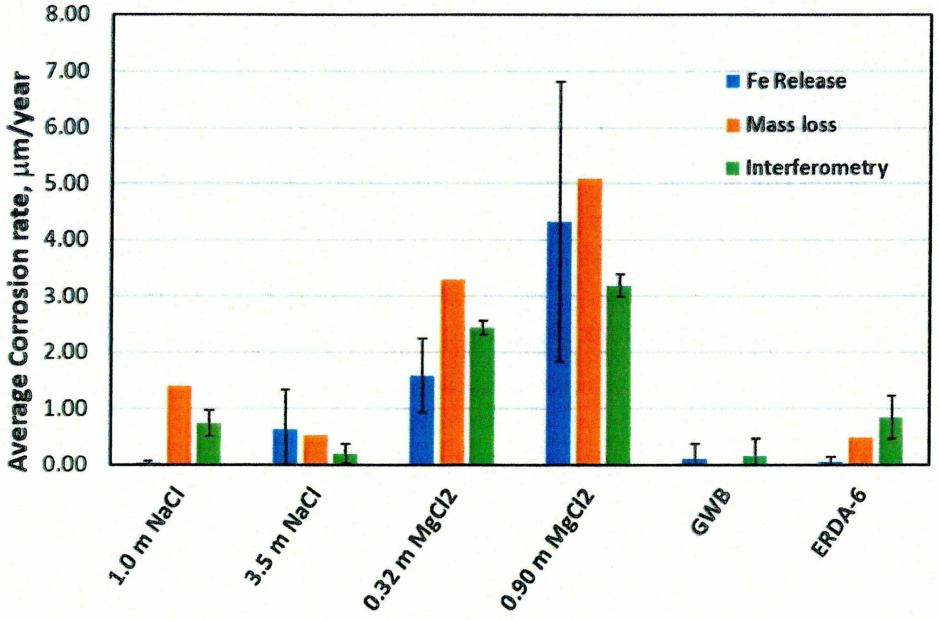

Figure 13. Average corrosion rates of C1018 by Fe release, mass loss and interferometry from the 6-month SPFT experiments with different brine solutions at 90 °C.

Information Only

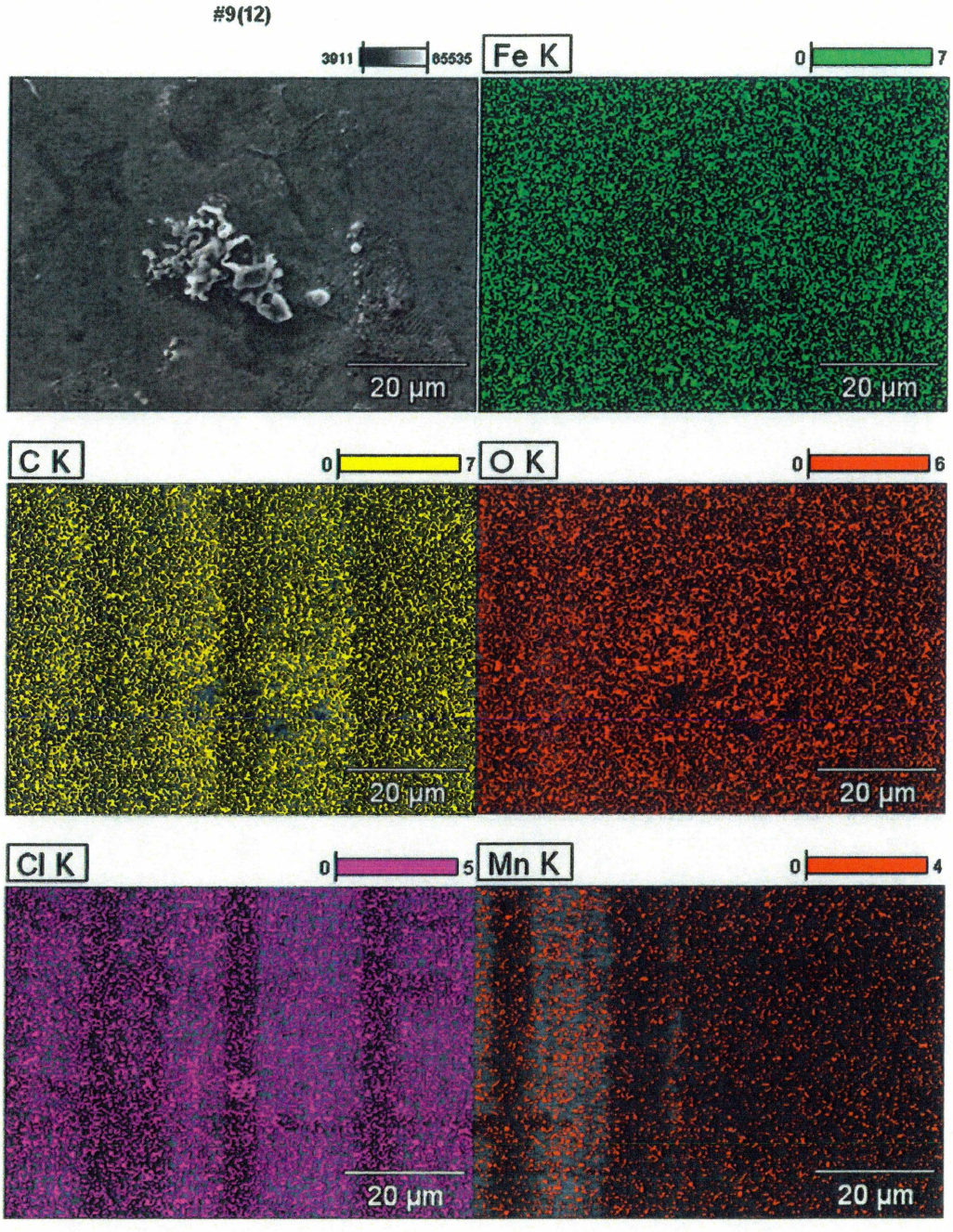

Figure 14. SEM Images of the Fe coupon surface from the 6-month SPFT experiment in GWB at 90 °C.

Information Only

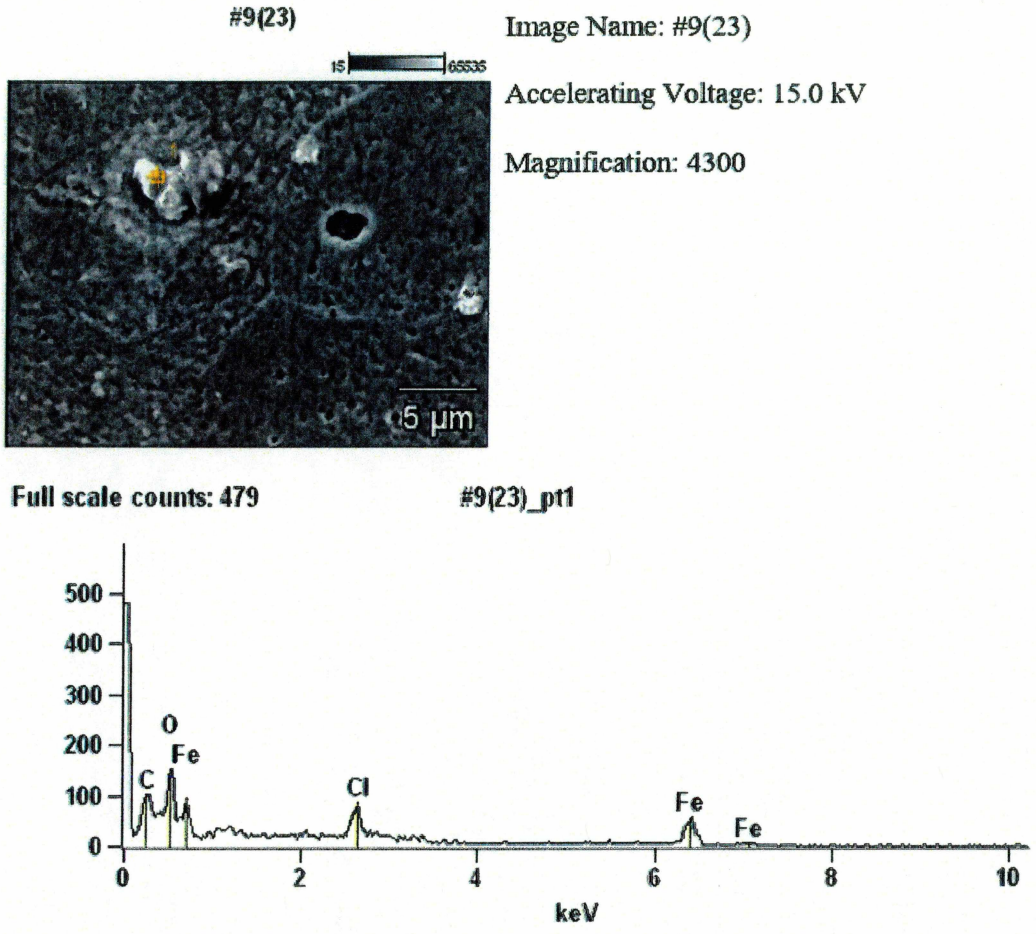

Figure 15. SEM Image and EDS analysis of the Fe coupon surface removed from the 6-month SPFT experiment in GWB at 90 °C and EDS analyses of solid particles on the surface.

Information Only

4. STATIC REACTION METHOD

4.1. Method and Corrosion Rates

4.1.1. Experimental setup

Static corrosion experiments were constructed to compare corrosion rate and possible corrosion products with those generated by the SPFT experiments. Static experiments were performed in a closed system, so the reactors will self-pressurize due to the generation of hydrogen gas. Monitoring of the pressure build-up can be used to determine gas generation rates during corrosion. A description of this method and experimental setup can be found in the FY20 milestone report (Zhang, 2020).

Inside the glovebox, C1018 steel disks (diameter = 1/2", thickness = 1/4") were placed inside thick walled glass tubes with a PTFE liner (i.e., the reactor). They were then immersed in about 40 mL of test brine and sealed. The reactors were then removed from the glovebox and placed into an aluminum block over a thermo dry bath. The heating element is set to a target temperature (e.g., 90 °C) with a thermocouple feedback to keep a constant temperature. The pressures inside of the reactors were monitored and recorded automatically every 10 minutes using a calibrated gauge in order to determine corrosion rate from gas (H_2) evolution over time.

4.1.2. Corrosion rate by H_2 generation

In this static experimental setup, the gas phase contains nitrogen, water vapor and H_2, along with other gas phases depending on the brine solution components, such as sulfide. The presence of these components could produce volatile gases during corrosion tests. In iron corrosion in brine solutions without additional source of other gas, the H_2 generation rate (over time) is proportional to Fe corrosion rate in the brine. The H_2 generation rate can be obtained by monitoring the pressure change vs. time, i.e. $\Delta P_{H2}/\Delta t$. The measured pressure increase is assumed to be due to the generation of hydrogen during the corrosion process. At termination of the static experiments, gas samples were collected from the headspace in the reactor and analyzed by gas chromatography (GC) to validate the H_2 generation rate and its concentration in the gas phase. Since the vapor pressure of water at a fixed temperature was unchanged during the static experiments, the total pressure change vs. time is equal to the H_2 pressure change vs. time, i.e. $\Delta P_{H2}/\Delta t = \Delta P/\Delta t$, which is the slope of the pressure recording vs. time. Once the $\Delta P/\Delta t$ (in psi/day) is measured by the static experiments, by assuming iron oxidizes solely to ferrous ion (i.e., Fe^{2+}) under the conditions explored in this study, the corrosion rate of Fe can be determined by the following equation (it should be noted that this calculated rate is an average corrosion rate over the period of experimental time, not an instantaneous measurement of corrosion rate):

$$r = \left(\frac{\Delta P}{\Delta t}\right)\frac{V}{RT} \times \frac{F_w}{\rho A} \times 248.3686 \quad (4)$$

where

r – Corrosion rate, μm/year

$(\Delta P/\Delta t)$ – Pressure change vs time, psi/day

V – Volume of head space, mL

R – Gas constant, 0.08206 atm·L/(mol·K)

Information Only

T – Temperature, K

F_w – Formula weight of testing material, g/mol (55.85 g/mol for C1018)

A – Exposed surface area of the coupon, cm^2

ρ – Density of tested materials, g/cm^3 (7.87 g/cm^3 for C1018)

The coefficient in Equation (4) is obtained by a conversion factor of units: pressure (1 atm = 14.6959 psi), time (1 year = 365 days), length (1 cm = 10^4 μm), and volume (1 mL = 10^{-3} L). The conversion is $365\times10^4\times10^{-3}/14.6959 = 248.3686$. The minimum resolvable daily change in pressure is 0.001 psi via this technique, corresponding to a minimum detectable corrosion rate of 0.09 μm/year.

4.2. Results by Static Method and Discussion

The static iron corrosion experiments were not completed when the FY20 milestone report was published and part of pressure data was collected (Zhang, 2020). All gas generation pressure data from the static corrosion experiments will be summarized in a FY22 milestone report and analyzed in another AR.

Information Only

5. ELECTROCHEMICAL METHOD

5.1. Method and Corrosion Rates

5.1.1. Experimental setup

A 3-electrode technique was implemented for measuring corrosion rates: reference electrode (RE): saturated calomel electrode (SCE) through a bridge tube filled with the testing brine solution), counter electrode (CE): platinum wires, and working electrode (WE): C1018. A description of this method and lab setup can be found in the FY20 milestone report (Zhang, 2020).

Electrical Impedance Spectroscopy (EIS) tests were run every few hours (e.g., 2-4 hours) for a certain period of time in each test depending on the stability of the corrosion experiments (all tests reported in this document were 72 hours). Polarization resistance, R_p, can be determined from the EIS measurements. At the end of the EIS tests, a Potentiodynamic Polarization (PDP) test was conducted to determine the Tafel slope of both anodic and cathodic reactions for calculating the corrosion rates.

5.1.2. Corrosion rate by electrochemical tests

In order to calculate corrosion rate in μm/year the corrosion current density (i_{corr}) must be determined. It is determined by the R_p and the Stern-Geary coefficient, B, from EIS and PDP tests, respectively:

$$i_{corr} = \frac{B}{R_P} \tag{5}$$

where

i_{corr} – Corrosion current density, A/cm^2

B – Stern-Geary coefficient, V/decade, defined by Eq. (6).

R_P – Polarization resistance, Ohm·cm^2

Figure 16(a) shows typical of EIS spectra (Bode phase angle and magnitude) from an electrochemical test. The polarization resistance, R_p, was obtained by fitting the EIS data to an appropriate equivalent circuit model based on the tested material (metal) and its environments (e.g., brine solution) (Zhang et al., 2021). Once an appropriate circuit analog/model was identified, the model was fit to the measured data via the Echem Analyst software package (Gamry-Instruments, 2011), allowing determination of the polarization resistance, R_p, from each EIS experiment. A PDP test is a DC corrosion experiment where the applied potential is swept at a fixed rate between two potentials while measuring the resulting current. In these experiments, the initial and final potentials represented potentials slightly more positive than and slightly more negative than the open circuit potential (OCP), and the potential was swept from below to above the OCP (i.e. from cathodic to anodic), as shown in **Figure 16(b)**. Once the PDP test was completed, a plot of applied potential vs. current density (at logarithmic scale) is generated and fitted to obtain the Tafel slope of anodic and cathodic reactions (Zhang et al., 2021). The Stern-Geary coefficient, B, can be determined from the PDP test and used in calculating the corrosion current density (Kelly et al., 2003).

Information Only

$$B = \frac{\beta_a \beta_c}{2.303(\beta_a + \beta_c)} \quad (6)$$

where β_a and β_c, in V/decade, the Tafel slope of anodic and cathodic reactions, respectively.

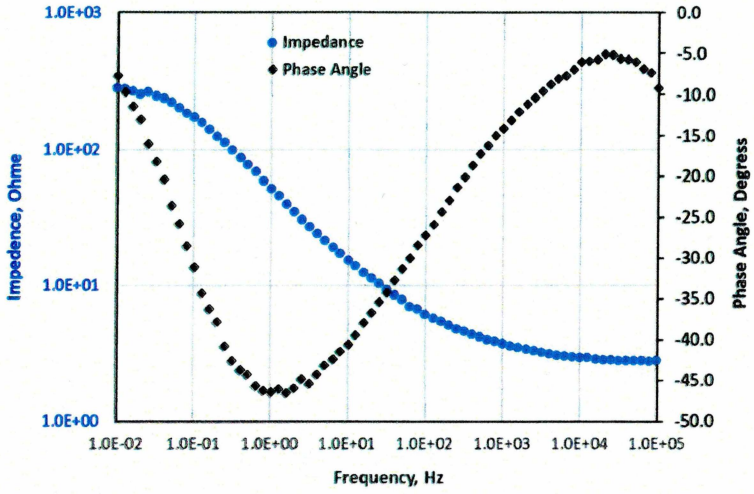

(a)

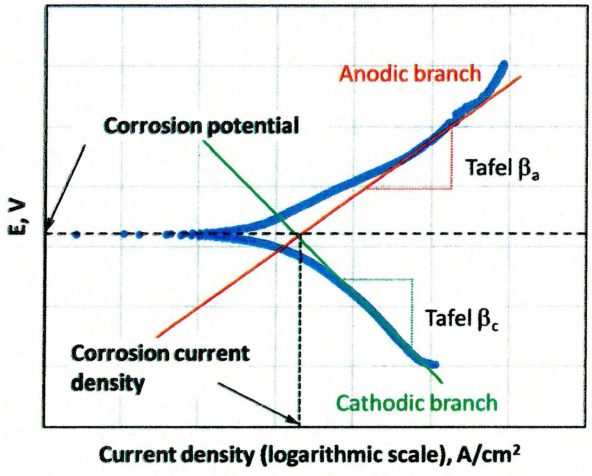

(b)

Figure 16. (a) A typical EIS spectra and phase angles from electrochemical cell test, (b) Tafel extrapolation from a potentiodynamic polarization test.

Once the corrosion current density i_{corr}, in µA/cm^2, is calculated using Equation (5), it can be converted into the corrosion rate, in µm/year, using this equation:

$$r = \frac{315{,}360 \times F_w}{nF\rho} \times i_{corr} \quad (7)$$

where

r – Corrosion rate, µm/year

ρ – Density of tested material, g/cm^3 (7.87 g/cm^3 the C1018)

Information Only

F_w – Formula weight of testing material, g/mol (55.85 g/mol for C1018)

n – Mole of electrons for anodic reaction (n=2 for Fe, assuming ferrous ions dominant)

F – Faraday constant, 96485 C/mol

i_{corr} – Corrosion current density, μA/cm^2

Equation (7) gives a conversion factor of 11.6 (i.e. 1 μA/cm^2 = 315,360×55.85/(2×96485×7.87) = 11.6 μm/year) for the tested material steel C1018.

5.1.3. Data Analysis of Electrochemical Measurements

The EIS and PDP tests were performed for iron corrosion by the electrochemical method using the Gamry Interface 1010E as per SP 12-40, *Calibration and Use of the Gamry Interface 1010E Potentiostat/Galvanostat*. The analysis of EIS spectra and the Tafel fitting of PDP measurements were done using the Echem Analyst™ Software Version 7.07 (Gamry-Instruments, 2011). An analysis plan (AP) AP 189 Rev. 0 was used for data analysis of EIS and PDP measurerments for corrosion rates (Zhang et al., 2021).

5.2. Results by EIS/PDP Tests and Discussion

5.2.1. EIS and PDP tests

A series of six electrochemical tests were performed on the C1018 in the SGWB solution, consisting of 3.2 m NaCl and 0.90 m $MgCl_2$, at 90 °C. The SGWB bine was selected for initial experiments. Other brine solutions such as NaCl, $MgCl_2$, GWB and ERDA-6 will be included in the future electrochemical experiments. The working electrode (sample holder, with an exposed surface area of 0.785 cm^2) was loaded with a C1018 coupon, which was polished to a 0.3 μm grit finish confirmed by interferometry (see Appendix A in the milestone report by Zhang (2020)). Two different experimental configurations were used – three samples were evaluated in SGWB where the solution was sparged with N_2 throughout the test (called Test #1-3: N_2 bubbling in solution) and three samples were evaluated in SGWB where the headspace over the solution was N_2 (i.e., no sparging, called Test #4-6: N_2 filling in headspace). The specifications for these electrochemical experiments are summarized in **Table 8**.

Table 8. A summary of electrochemical experiments for the C1018 coupons in the SGWB solution at 90 °C

Test Date	Test #	Coupon ID	Brine Solution	UHP N_2 flowrate (degassing), L/min	N_2 Line Position
3/13/2020	1	C1018-1	SGWB	0.1	Bubbler in solution
3/20/2020	2	C1018-2	SGWB	0.1	Bubbler in solution
3/26/2020 [a]	3	C1018-3	SGWB	0.1	Bubbler in solution
4/08/2020	4	C1018-4	SGWB	0.1	Line in headspace
4/13/2020	5	C1018-5	SGWB	0.1	Line in headspace
4/20/2020	6	C1018-6	SGWB	0.1	Line in headspace

[a] A failing glass frit was found during this experiment (after 20 hours)

Information Only

The EIS spectra for each test are shown in **Figure 17** (N_2 bubbling in solution) and **Figure 18** (N_2 in headspace). It should be noted that due to a failing glass frit in the experimental setup when acquiring data on 3-26-20 (Test #3), significant noise was present in the impedance spectrum for frequencies between 10 and 700 Hz (after 20 hours). The data above 700 Hz do show the similar trend of EIS and phase angles at time frames prior to 20 hours, only data below 10 Hz are presented in **Figure 17** for the polarization resistance, R_p, which was determined by following AP-189 by fitting the EIS to an appropriate equivalent circuit model.

Each of PDP tests was performed when an EIS measurements were completed at 72 hours. All data are plotted in **Figure 19(a)** (N_2 bubbling in solution) and **Figure 19(b)** (N_2 filling in the headspace). Due to strong noise from Test #3, the PDP data is not shown in **Figure 19(a)**.

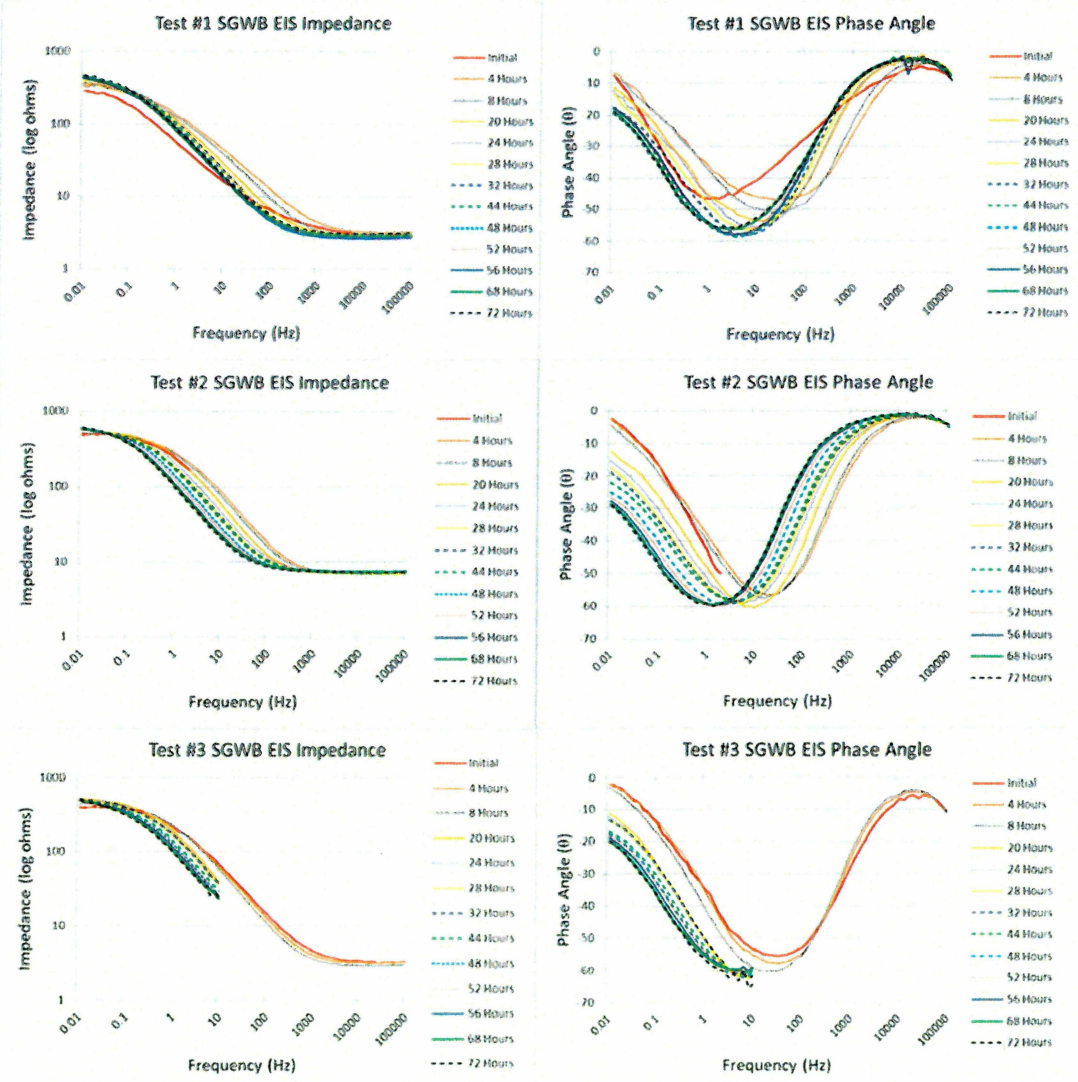

Figure 17. EIS spectra and phase angles of C1018 coupons in the SGWB brine with N_2 bubbling in solution at 90 °C.

Information Only

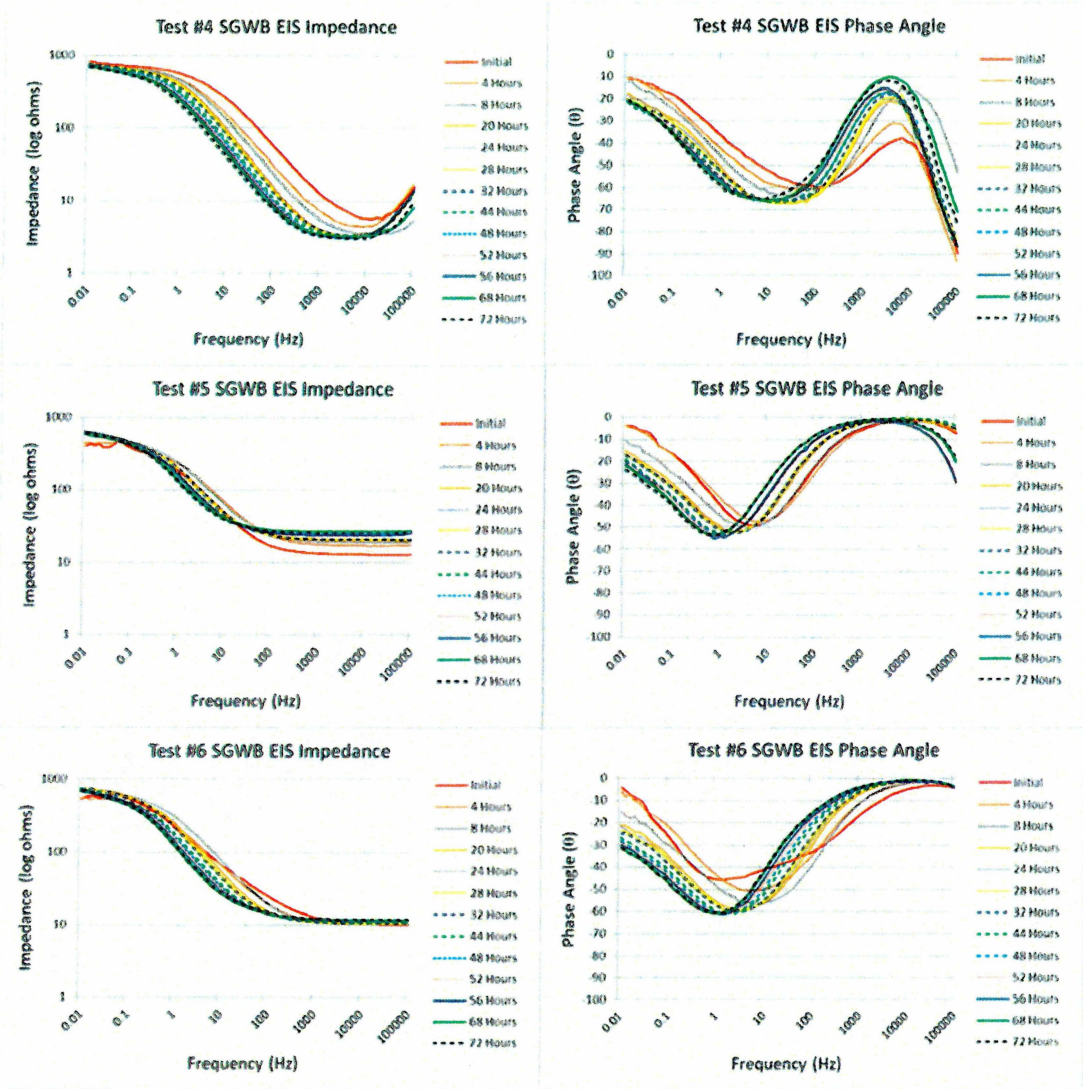

Figure 18. EIS spectra and phase angles of C1018 coupons in the SGWB brine with N_2 in headspace at 90 °C.

Information Only

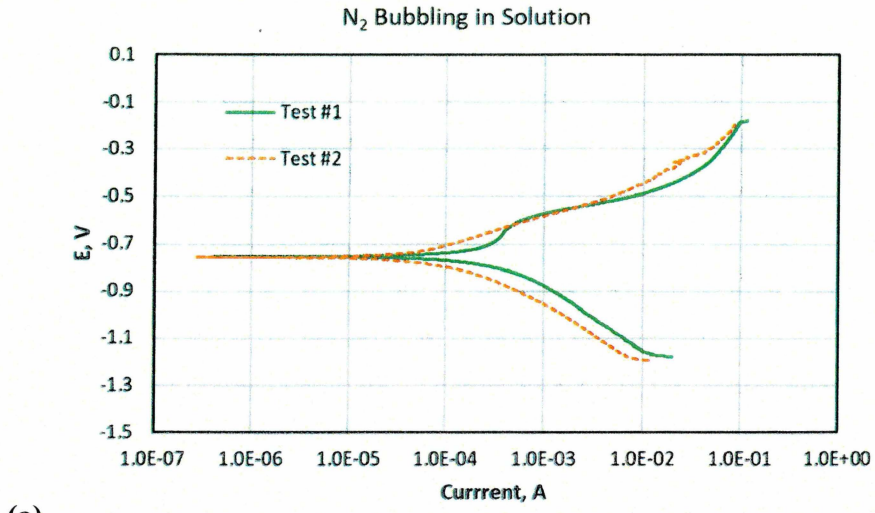

(a)

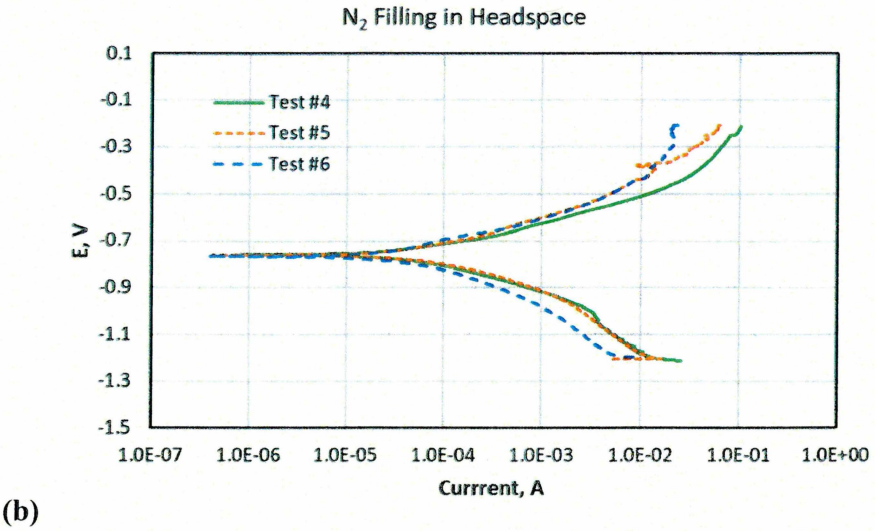

(b)

Figure 19. PDP data of C1018 coupon in the SGWB brine with (a) N_2 bubbling in solution, (b) N_2 filling in headspace at 90 °C.

5.2.2. Corrosion rates

The analysis plan AP-189 Rev. 0 describes how polarization resistance, R_p, and corrosion rate are determined from the EIS and PDP measurements (Zhang et al., 2021). The polarization resistances, R_p, extracted from the EIS measurements by fitting them to the rotated disk equivalent circuit model. All fitted R_p values, averages and standard deviations are presented in **Table 9**. The Tafel constants (β_a and β_c) extracted from PDP measurements and the Stern-Geary coefficient (B) calculated using Equation (6) are also presented in **Table 10**.

With the estimated polarization resistance (R_p) and the Stern-Geary coefficient (B) listed in **Table 9** and **Table 10**, corrosion rates for each test were determined using Equation (7).

Information Only

Table 9. A summary of polarization resistances (Ohm), R_p, estimated by EIS measurements for the C1018 coupons in the SGWB solution at 90 °C

Time, hours	Test# (N_2 bubbling in solution)			Ave.	Std. Dev.	Test# (N_2 filling in headspace)			Ave.	Std. Dev.
	1	2	3			4	5	6		
0	373	451	418	414	39	850	419	730	666	223
4	366	506	406	426	72	815	447	587	616	185
8	350	533	463	449	92	771	587	750	703	101
20	362	596	659	539	157	754	622	831	736	106
24	368	627	636	544	152	772	657	849	759	97
28	408	643	598	550	125	784	675	841	767	85
32	458	648	563	556	95	794	682	856	777	88
44	483	656	564	568	86	803	690	866	786	89
48	468	702	574	581	117	801	727	883	803	78
52	480	739	536	585	136	757	745	901	801	87
56	454	774	560	596	163	761	755	918	811	92
68	521	812	618	650	148	734	719	925	792	115
72	551	829	582	654	152	744	746	941	810	113

Table 10. A summary of Tafel slopes β_a and β_c (V/decade) and the Stern-Geary coefficient B estimated by PDP measurements for the C1018 coupons in the SGWB solution at 90 °C

Time, hours	Test# (N_2 bubbling in solution)			Ave.	Std. Dev.	Test# (N_2 filling in headspace)			Ave.	Std. Dev.
	1	2	3 *			4	5	6		
β_a	0.1941	0.1784	-	0.1863	0.011	0.1683	0.1878	0.2077	0.1879	0.020
β_c	0.2129	0.2175	-	0.2152	0.003	0.2006	0.2029	0.2221	0.2085	0.012
B **	0.1941	0.1784	-	0.1863	0.011	0.1683	0.1878	0.2077	0.1879	0.020

* PDP for Test#3 has strong noise and is not included in the data analysis. The average Tafel constants from Test#1 and #2 were used to calculate the corrosion rates.

** The Stern-Geary coefficient was calculated using Equation (6).

Table 11 summarizes all corrosion rates and the triplicate averages/standard deviations for the C1018 Coupons in the SGWB solution at 90 °C. The average corrosion rates over time (with Std. Dev. displayed) by triplicate tests are also plotted in **Figure 20** at two experimental conditions: (a) N_2 bubbling in solution and (b) N_2 filling in headspace.

There was a decrease in the corrosion rate and variability in results between the first (bubbling in solution, 796 μm/year at 72 hours) and the second (filling in headspace, 617 μm/year at 72 hours) triplicate tests. The only differing factor between two sets of tests was the position of the N_2 gas line. Tests #1-3 had the nitrogen continuously bubbling inside of the solution. Even though the rate was as low as about 0.1 L/min, it is apparent that even a small stirring of solution by N_2 bubbling has an impact on corrosion rate. It appears that the rate was affected by the gentle bubbling, which could possibly affect the mass transport and/or surface diffusion of ions resulting from corrosion reactions. Test #4-6 were run with the nitrogen gas line inside of the cell headspace.

Information Only

This ensured the cell remained oxygen free with less disturbance to the solution. The corrosion rates over time are smaller than those with N_2 bubbling in the solution. One of possible reasons is the mass transport of ions between the bulk solution and the coupon surface.

Overall, the corrosion rates determined by the electrochemical method are much higher than those by the SPFT method. It could be due to different experimental condition for these tests (e.g., pH of SGWB is 6.6). More experiments are needed to verify if/how a passivation layer is formed on the Fe coupon surfaces, which could slow down overall corrosion in the tested brines.

EIS and PDP measurements in this study were performed in the SGWB brine degassed by N_2 in a lab where no glovebox was available. There was no control of the oxygen level in brine solutions even though a stream of N_2 was used for degassing the solution. The possible oxygen in brine solution may be one of the reasons why the corrosion rates from EIS and PDP measurement in this study is much higher than those from SPFT. Another reason could be the surface roughness (0.3 μm) of the C1018 coupons (polished in the lab, see Appendix A in the FY20 milestone report (Zhang, 2020) used in EIS and PDP measurements is one order of magnitude higher than those mirror-like coupons (surface roughness: 0.03 μm) polished in SNL Metallurgy and Materials Joining Department (Org. 01831).

The corrosion rates of iron in SGWB obtained via the electrochemical method two orders of magnitude higher than that in 0.9 m $MgCl_2$ obtained via SPFT experiments, where the corrosion rate remains relatively constant over the course of the 6-month tests. These high corrosion rates may suggest the initial polarization potential used in the PDP experiments (-500 mV relative to open circuit) may have resulted in electrochemical parameters (i.e., Tafel slopes) that were not representative of the behavior at OCP, leading to a higher corrosion rates. The parameters for EIS/PDP tests should be adjusted such that an appropriate PDP curve can be achieved. For example, a smaller polarization potential relative to open circuit may be used in PDP tests for the Tafel constants, preventing the unintended reduction of the oxide layer on the steel surface, altering the electrochemistry.

As mentioned above, pH of brine solution, surface roughness of the coupon, and possible dissolved oxygen (DO) applied for EIS/PDP tests are different from those used in SPFT experiments. Preliminary results from a second set of EIS/PDP experiments performed after 50-hr at 90 °C with the same SGWB brine degassed instead inside a glovebox showed that Fe corrosion rates would be reduced 2-4 times, indicating that the DO in the brine may not be properly removed by degassing with N_2 at ambient condition (without glovebox). A glovebox (oxygen level is less 5 ppm) will be used to perform the EIS and PDP measurements for the mirror-like polished C1018 coupons so that test conditions (surface roughness of C1018 coupons, oxygen level in brine solutions) for EIS and PDP measurements would be comparable to those in SPFT experiments. In addition, long-term experiments (1~3 months) are planned for the future EIS/PDP measurements.

All files associated with data analyses in the analysis report are located at: cvs/CVSLIB/WIPP_EXTERNAL/AP189

Information Only

Table 11. A summary of corrosion rates (μm/year) by the electrochemical method for the C1018 coupons in the SGWB solution at 90 °C

Time, hours	Test# (N_2 bubbling in solution)			Ave.	Std. Dev.	Test# (N_2 filling in headspace)			Ave.	Std. Dev.
	1	2	3			4	5	6		
0	1373	1096	1201	1223	140	542	1173	741	819	323
4	1399	976	1239	1205	213	566	1098	921	862	271
8	1462	926	1085	1158	275	598	837	721	718	120
20	1414	828	763	1002	359	611	790	650	684	94
24	1388	788	790	989	346	597	748	637	661	78
28	1253	767	840	953	262	588	728	643	653	71
32	1118	762	892	924	180	581	721	632	644	71
44	1059	753	890	901	154	574	712	624	637	70
48	1093	704	876	891	195	575	676	612	621	51
52	1066	668	938	891	203	609	659	600	623	32
56	1127	638	897	887	245	606	650	589	615	32
68	982	608	813	801	187	628	684	585	632	50
72	928	596	864	796	176	620	658	574	617	42

Information Only

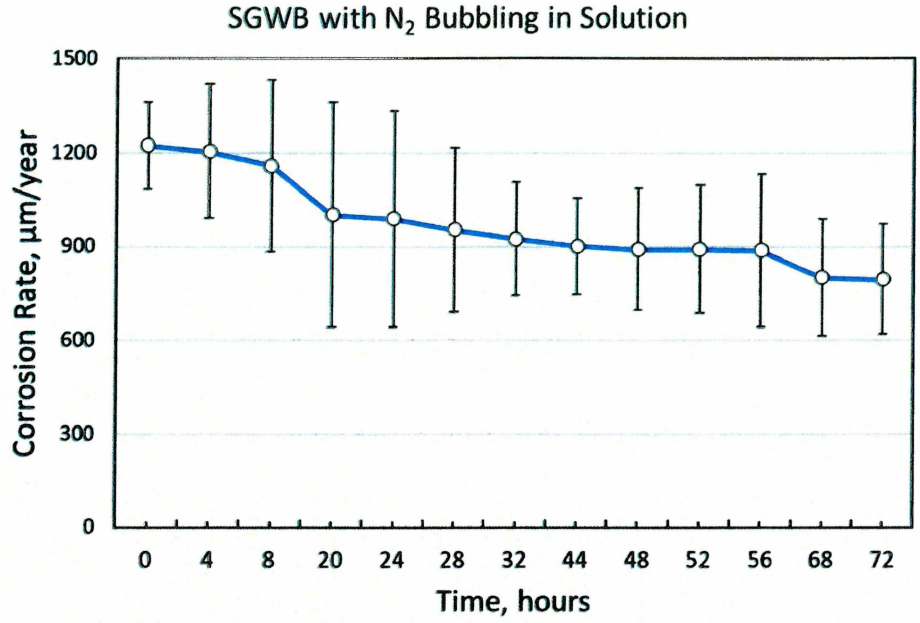

(a)

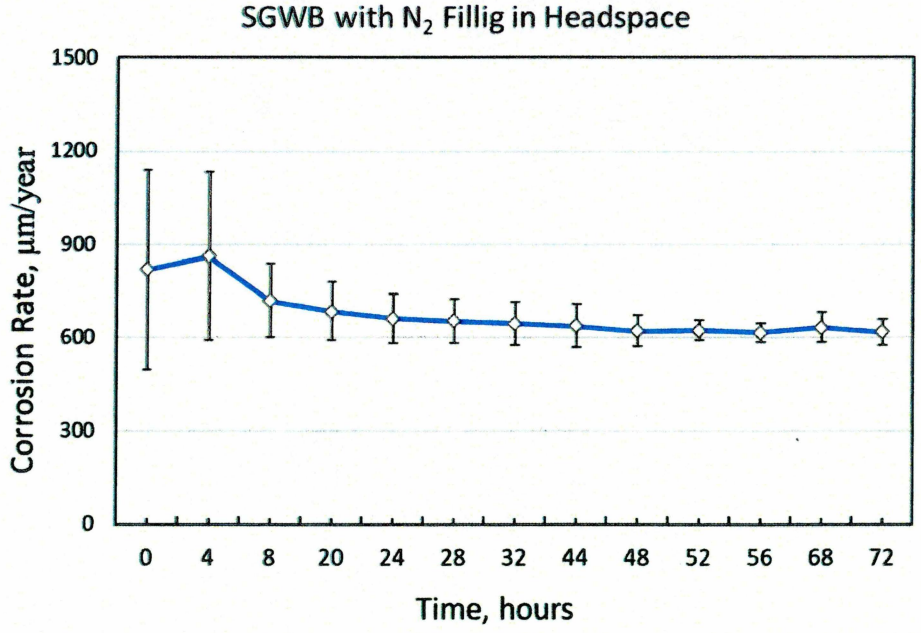

(b)

Figure 20. Corrosion rates of C1018 coupon vs. time in SGWB at 90 °C with (a) N_2 bubbling in solution, (b) N_2 filling in headspace. Error bars represent the standard deviations determined by triplicate measurements.

Information Only

6. SUMMARY

This report describes the results of iron corrosion experiments at 90 °C by the SPFT and electrochemical methods. Analysis of the data from both SPFT and EIS/PDP experiments gives the following preliminary results:

From the SPFT experiments, the corrosion rates in the same brine solution are slightly different by three analysis techniques (Fe release, mass loss and interferometry), particularly, in the brine with less corrosion (e.g., GWB), see Table 7 on page 33. The corrosion rates in brines with higher corrosion (0.32 m and 0.90 m $MgCl_2$) show smaller difference by the three techniques. The order of the corrosion rate vs. brine solution is 0.90 m $MgCl_2$ > 0.32 m $MgCl_2$ > 3.5 m NaCl > (1.0 m NaCl ~ ERDA-6 ~ GWB). Overall, mass loss yielded the largest corrosion rates, as expected given that it accounts for all mass change on the coupon. Fe release neglects the surface oxide layer, resulting in an underestimation of corrosion rate. The interferometry measures only on an extremely small portion of the sample surface and need more data to be compared with other techniques. This preliminary result is obtained from one set of SPFT experiments. For better statistic results, more SPFT experiments (and static corrosion tests) have been performed and data will be reported/analyzed in subsequent reports.

From electrochemical EIS/PDP measurements in the SGWB brine, the corrosion rate shows a decreasing trend and slowly approaches to a stable level. The disturbance of the brine solution by N_2 bubbling in solution and filling in headspace could affect the mass transport and/or surface diffusion of ions and further the corrosion rate. The corrosion rates determined by the electrochemical method are much higher than those by the SPFT method. More experiments are needed to verify if/how a passivation layer is formed on the iron coupon surfaces and slows overall corrosion in the tested brines.

Information Only

7. ACKNOWLEDGEMENTS

The authors would like to acknowledge Chase Kicker (a year-round student intern from New Mexico Tech) for performing the electrochemical experiments, Cassie Marrs, Jandi Knox, and Heather Burton (Org. 08882) for chemical analysis and characterization, and Christina Profazi (Org. 01831) for polishing the steel coupons in SPFT experiments.

Information Only

8. REFERENCES

ASTM. (2003). *G1-03: Standard Practice for Preparing, Cleaning, and Evaluating Corrosion Test Specimens*. ASTM International, West Conshohocken, PA.

Brush, L. H. (1995). *Systems Prioritization Method Iteration 2 Baseline Position Paper: Gas Generation in the Waste Isolation Pilot Plant*. Sandia National Laboratories, Albuquerque, NM. ERMS 228740.

Gamry-Instruments. (2011). *The Echem Analyst Software Guide*.

ISO. (1991). *8470: Corrosion of metals and alloys - Removal of corrosion products from corrosion test specimens.*

Kelly, R. G., Scully, J. R., Shoesmith, D. W., and Buchheit, R. G. (2003). *Electrochemical Techniques in corrosion Science and Engineering. Chapter 4: The Polarization Resistance Method for Determination of Instantaneous Corrosion Rates*. Marcel Dekker. New York, NY.

Kirkes, L. (2019). *Lead Inventory Impact on Gas Generation*. Sandia National Laboratories, Carlsbad, NM. ERMS 571255.

Roselle, G. T. (2009). *Iron and Lead Corrosion in WIPP-Relevant Conditions: Six Month Results*. Sandia National Laboratories, Carlsbad, NM. 546084.

Roselle, G. T. (2011). *AP-159 Revision 0: Analysis Plan for Determination of Gas Generation Rates from Iron/Lead Corrosion Experiments*. Sandia National Laboratories, Carlsbad, NM. 556297.

Sisk-Scott, C., and Icenhower, J. (2016). *Iron and Lead Corrosion in WIPP-Relevant Conditions; Test Plan TP 06-02. Rev. 3*. Sandia National Laboratories, Carlsbad, NM. ERMS 565448.

U.S. DOE. (2004). *Title 40 CFR Part 191: Compliance Recertification Application for the Waste Isolation Pilot Plant, Vol. 1-8*. U.S. DOE, WIPP, Carlsbad Field Office, Carlsbad, New Mexico. DOE/WIPP 2004-3231.

U.S. DOE. (2019). *Compliance Recertification Application 2019, Appendix GEOCHEM-2019, Implementation of Chemistry Conceptual Models. Sections GEOCHEM-1.2.5 and GEOCHEM-3.4.1*. U.S. DOE, WIPP, Carlsbad Field Office, Carlsbad, New Mexico. DOE/WIPP-19-3609, Rev. 0.

U.S. EPA. (1996a). *Title 40 CFR Part 191: Environmental Radiation Protection Standards for Management and Disposal of Spent Nuclear Fuel and Transuranic Radioactive Wastes*. U.S. EPA, Office of Air and Radiation, Washington D.C.

Information Only

U.S. EPA. (1996b). *Title 40 CFR Part 194: Criteria for the Certification and Recertification of the Waste Isolation Pilot Plant's Compliance with the 40 CFR Part 191 Disposal Regulations*. U.S. EPA, Office of Air and Radiation, Washington D.C.

Van Soest, G. D. (2018). *Performance Assessment Inventory Report – 2018*. Los Alamos National Laboratory, Carlsbad, NM. LA-UR-18-31882.

Zhang, L. (2020). *FY20 Milestone Report on TP 06-02 Rev. 3*. Sandia National Laboratories, Carlsbad, NM. ERMS 574285.

Zhang, L., Hora, P., Jang, J., Kirkes, L., and Miller, C. (2021). *AP-189 Revision 0: Analysis Plan for Determination of Iron/Lead Corrosion Rates by Electrochemical Tests Under TP 06-02*. Sandia National Laboratories, Carlsbad, NM. ERMS 575289.

Information Only

APPENDIX A

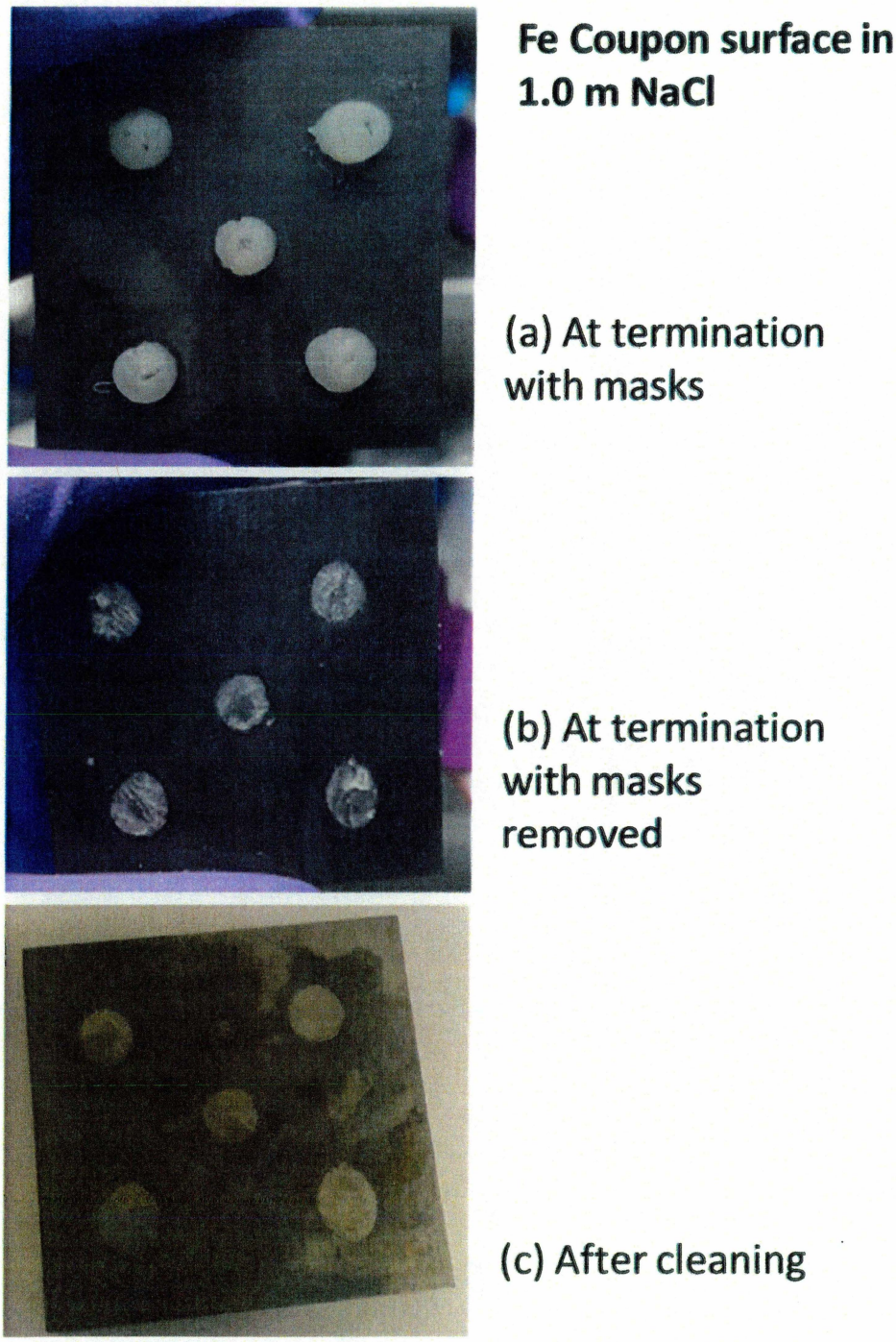

Figure A-1. Photos of Fe coupon surface in 1.0 m NaCl from a 6-month SPFT experiment at 90 °C: (a) termination with masks, (b) termination with masks removed, and (c) after surface cleaning.

Information Only

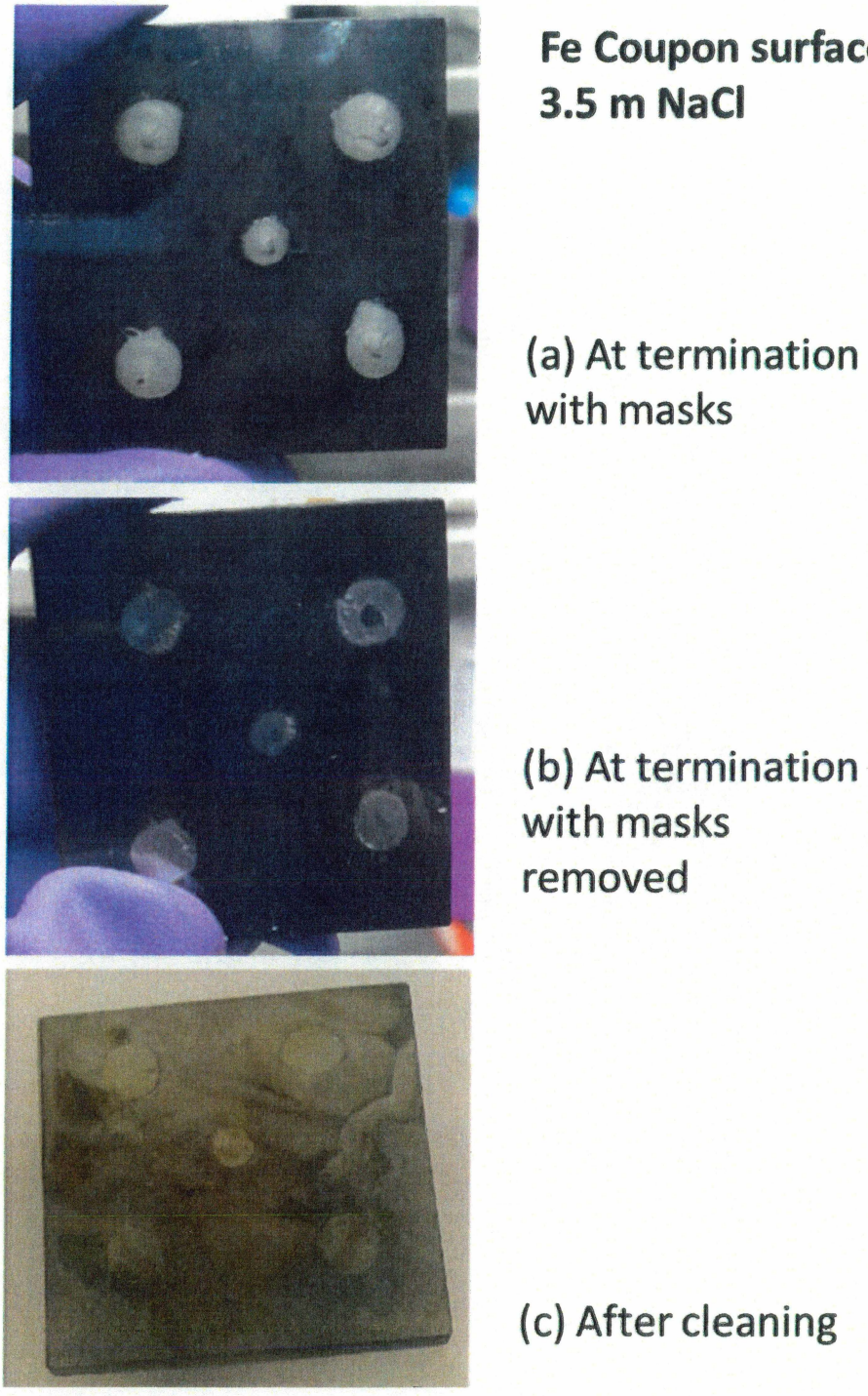

Figure A-2. Photos of Fe coupon surface in 3.5 m NaCl from a 6-month SPFT experiment at 90 °C: (a) termination with masks, (b) termination with masks removed, and (c) after surface cleaning.

Information Only

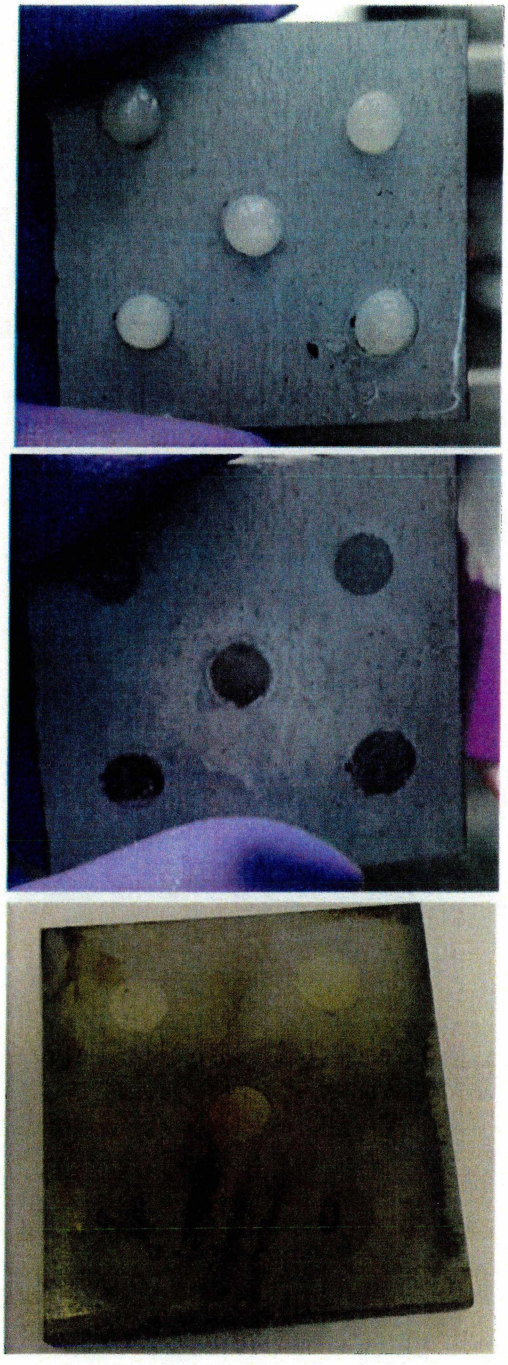

Figure A-3. Photos of Fe coupon surface in 0.32 m $MgCl_2$ from a 6-month SPFT experiment at 90 °C: (a) termination with masks, (b) termination with masks removed, and (c) after surface cleaning.

Information Only

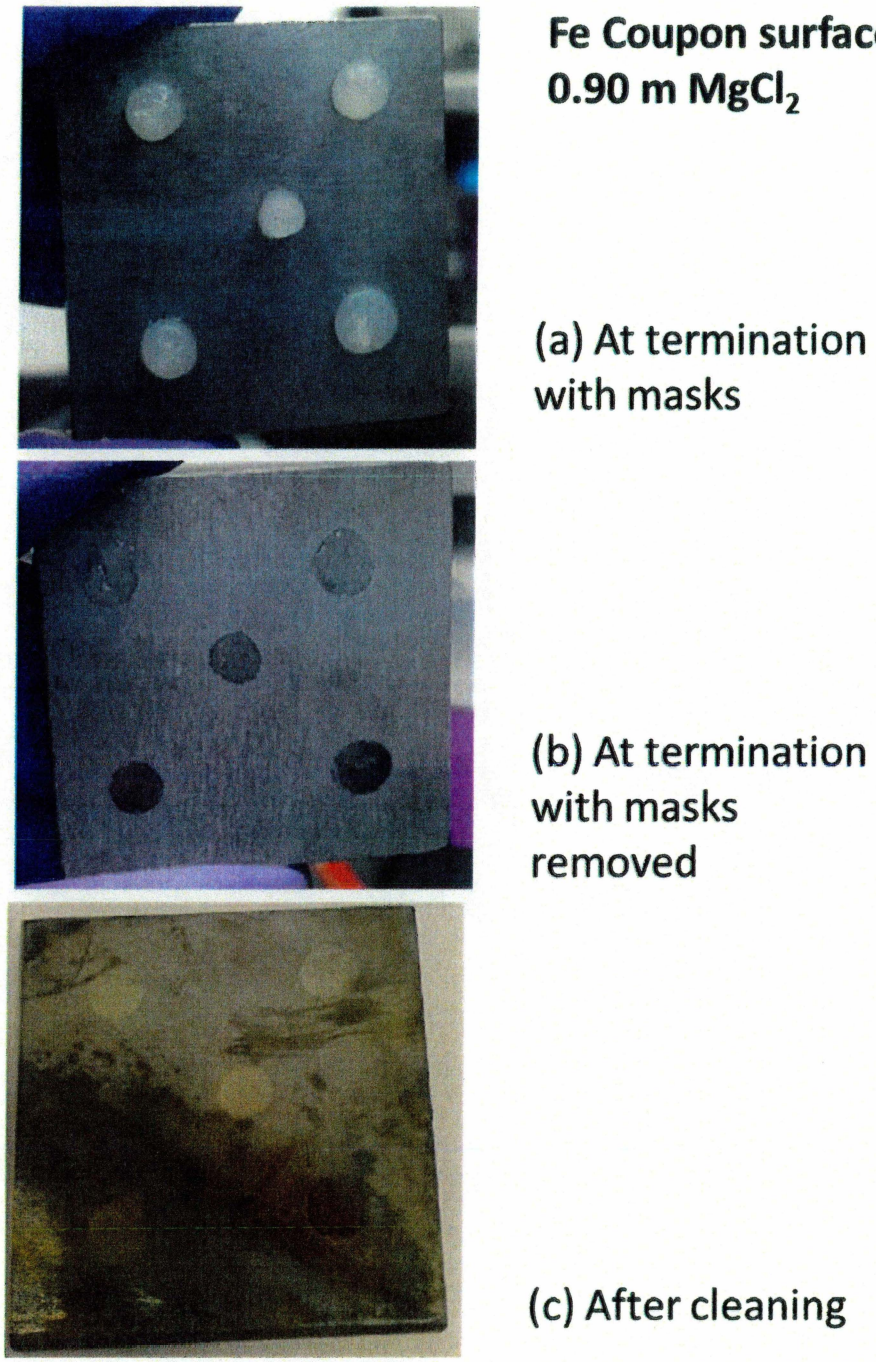

Figure A-4. Photos of Fe coupon surface in 0.90 m $MgCl_2$ from a 6-month SPFT experiment at 90 °C: (a) termination with masks, (b) termination with masks removed, and (c) after surface cleaning.

Information Only



Figure A-5. Photos of Fe coupon surface in GWB from a 6-month SPFT experiment at 90 °C: (a) termination with masks, (b) termination with masks removed, and (c) after surface cleaning.

Information Only

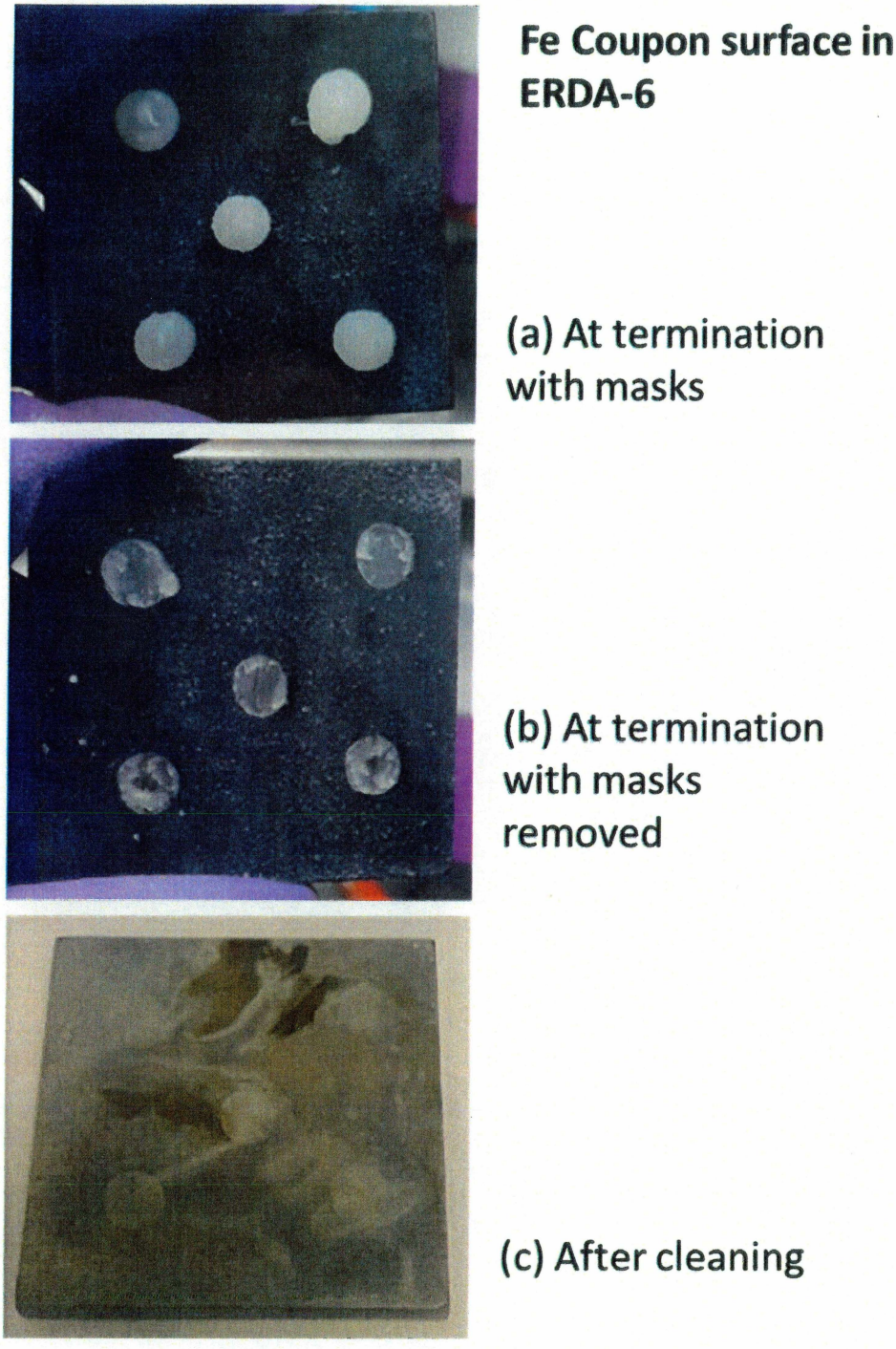

Figure A-6. Photos of the Fe coupon surface in ERDA-6 from a 6-month SPFT experiment at 90 °C: (a) termination with masks, (b) termination with masks removed, and (c) after surface cleaning.

Information Only

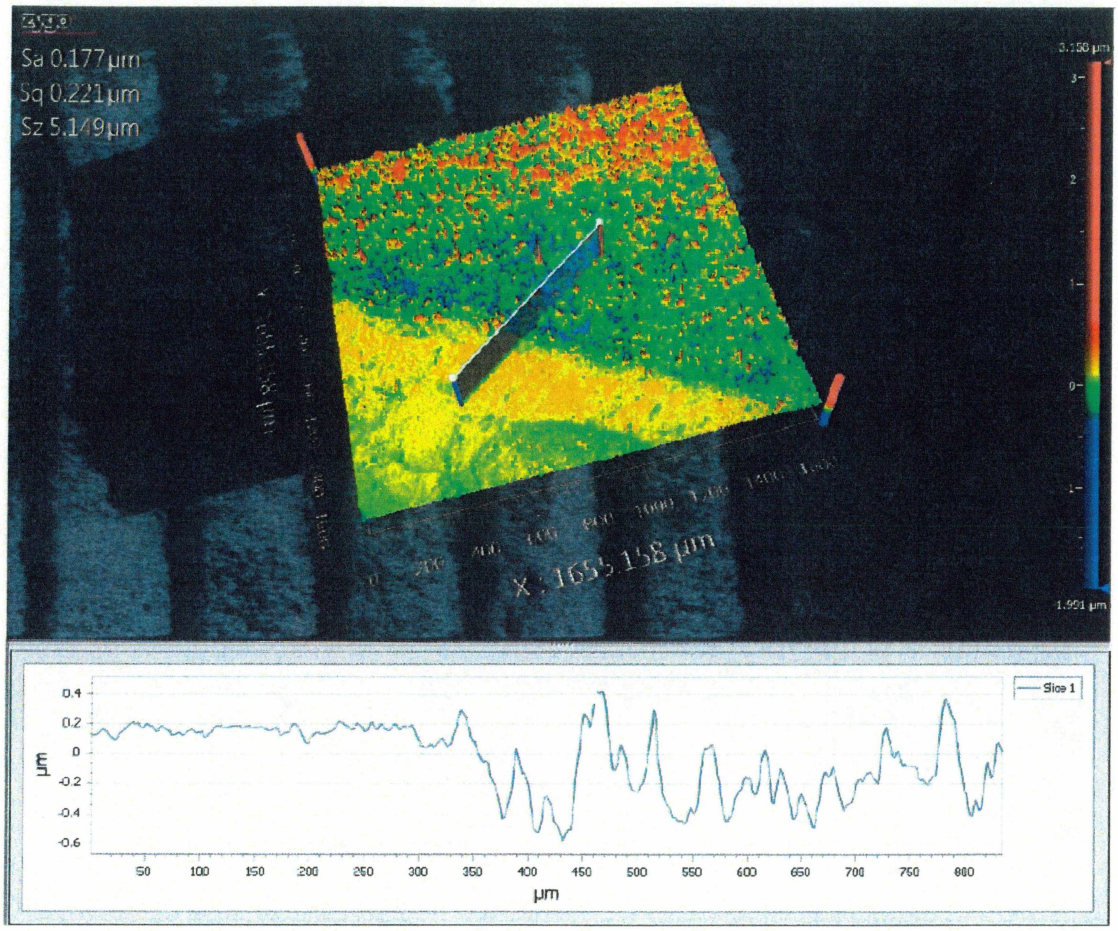

Figure A-7. Interferometry analysis of the Fe coupon surface in 1.0 m NaCl from the 6-month SPFT experiment at 90 °C.

Information Only

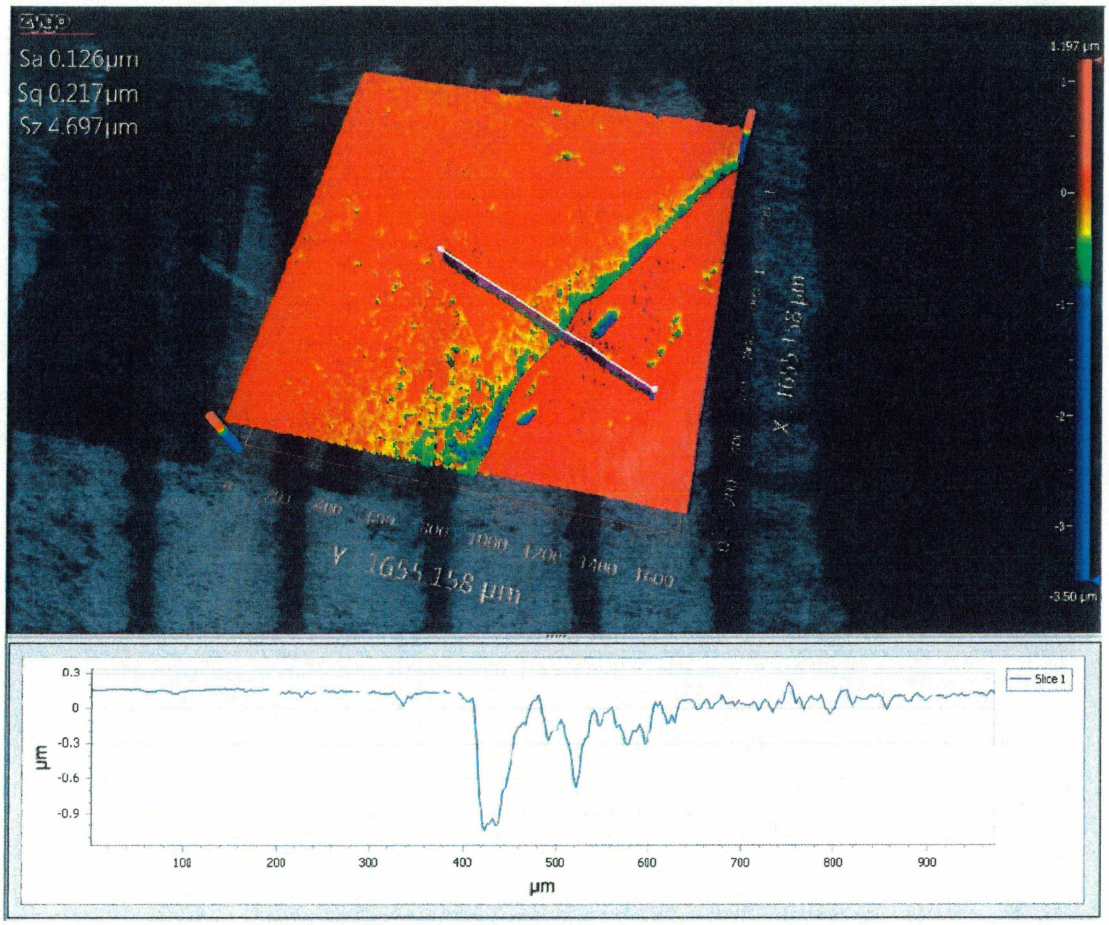

Figure A-8. Interferometry analysis of the Fe coupon surface in 3.5 m NaCl from the 6-month SPFT experiment at 90 °C.

Information Only

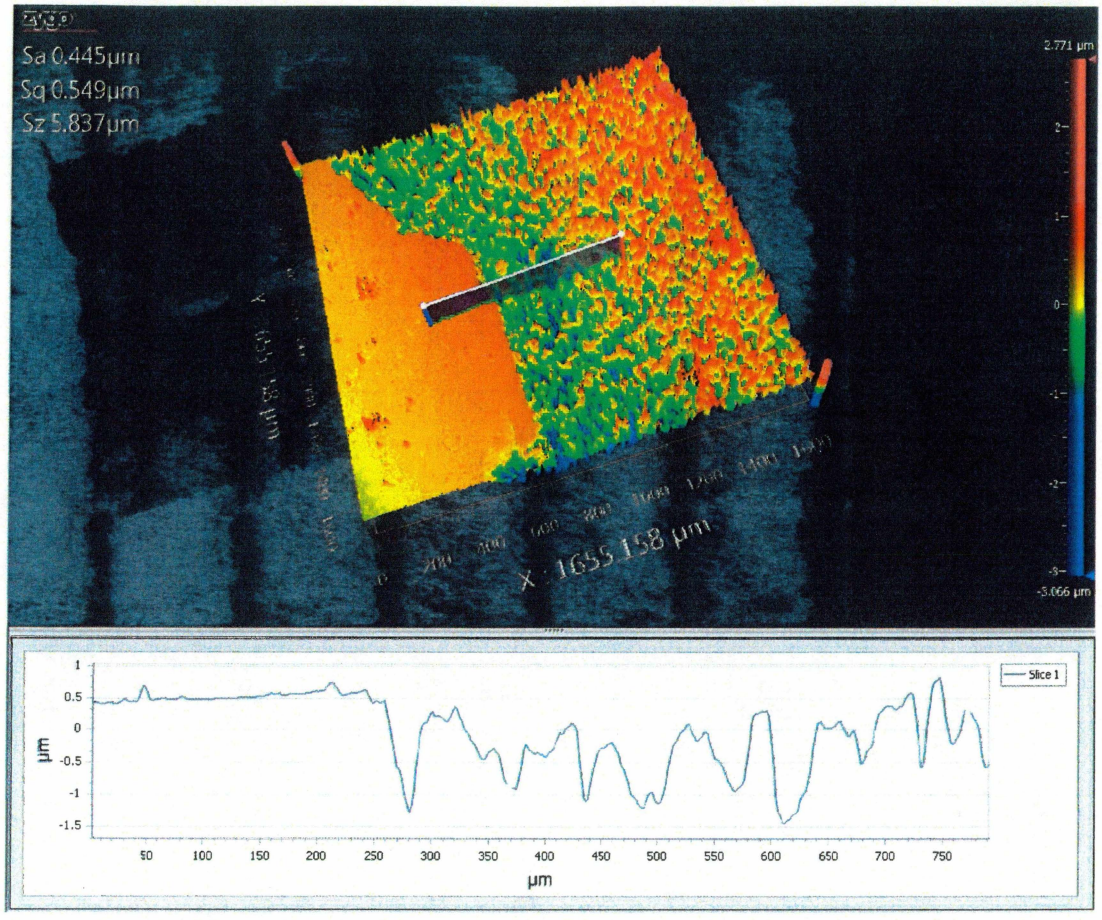

Figure A-9. Interferometry analysis of the Fe coupon surface in 0.32 m $MgCl_2$ from the 6-month SPFT experiment at 90 °C.

Information Only

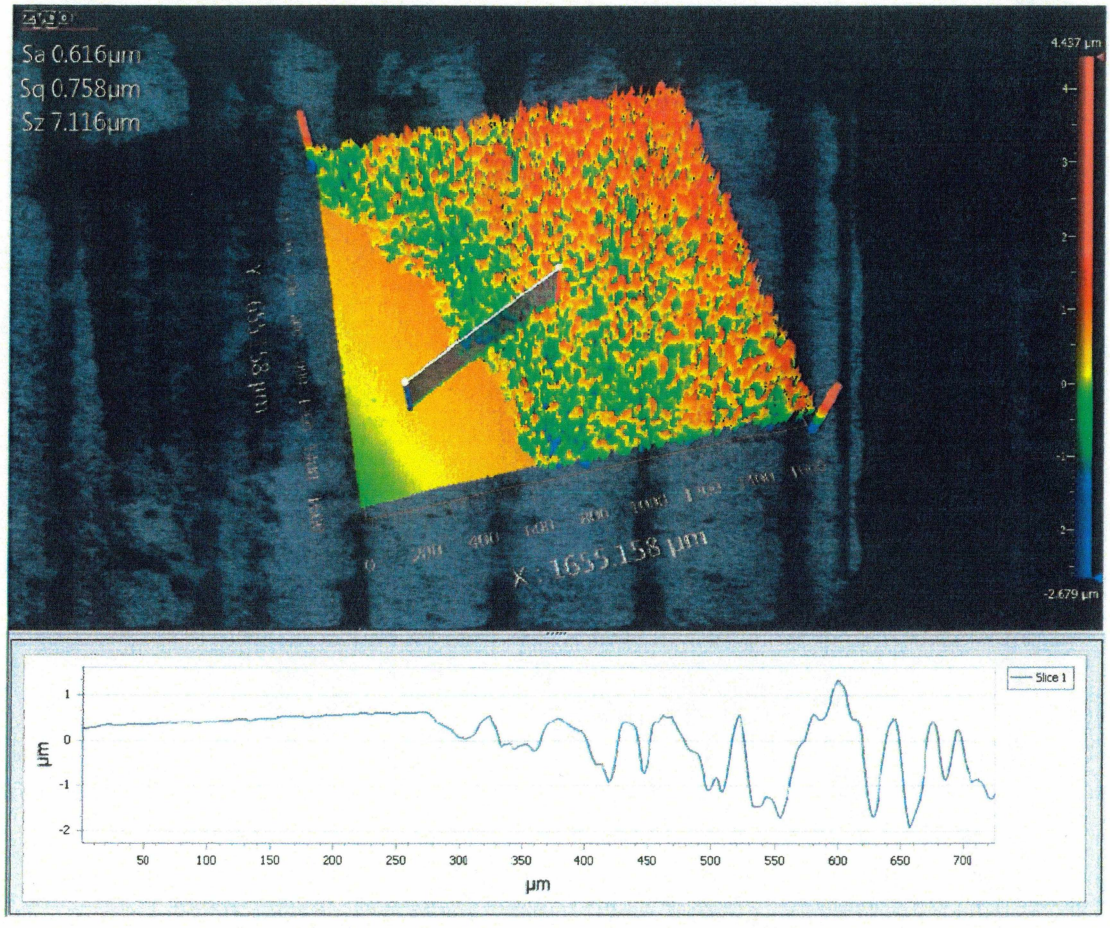

Figure A-10. Interferometry analysis of the Fe coupon surface in 0.90 m $MgCl_2$ from the 6-month SPFT experiment at 90 °C.

Information Only

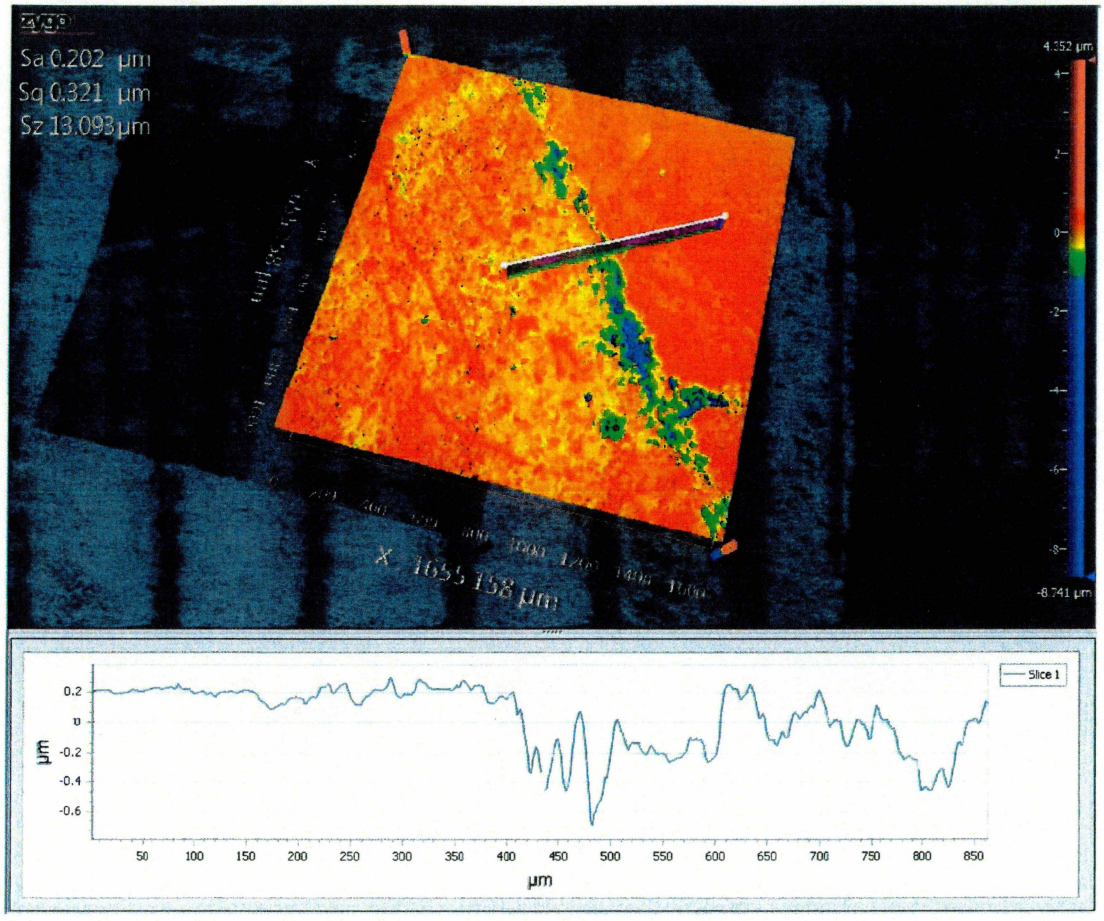

Figure A-11. Interferometry analysis of the Fe coupon surface in GWB from the 6-month SPFT experiment at 90 °C.

Information Only

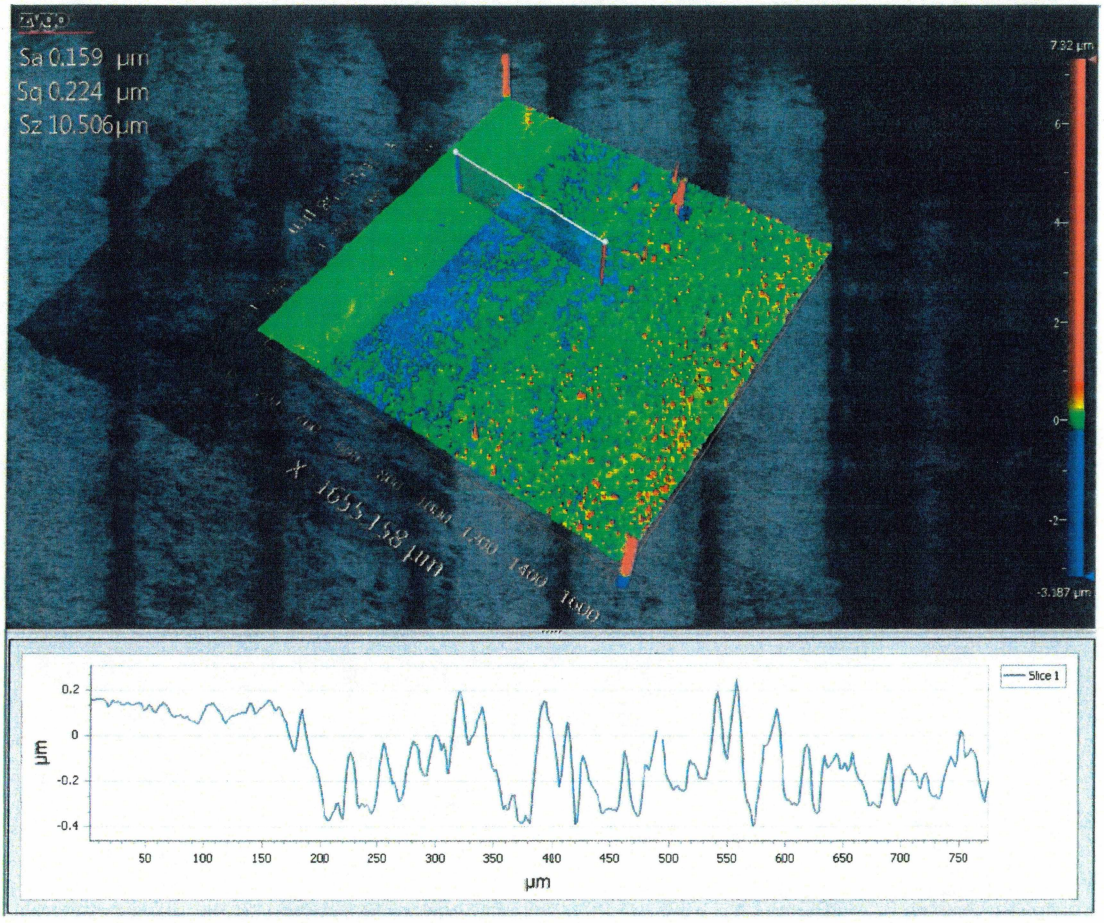

Figure A-12. Interferometry analysis of the Fe coupon surface in ERDA-6 from the 6-month SPFT experiment at 90 °C.

Information Only

APPENDIX B

Table B-1. Fe concentrations (ppb) in the effluent of each reactor from 6-month SPFT experiments at 90 °C [a]

Time, days	Week #	1.0 m NaCl	3.5 m NaCl	0.32 m $MgCl_2$	0.90 m $MgCl_2$	GWB	ERDA-6
0	0	-	-	-	-	-	-
8	1	87.93	5762.99	6521.44	63.82	2673.40	176.10
17	2	173.91	4602.19	4314.37	3037.51	427.20	1088.97
23	3	38.48	3360.34	6047.01	13181.09	111.49	115.12
30	4	263.78	1935.51	4356.46	14796.30	1225.22	41.30
37	5	205.33	1510.72	3472.01	7092.96	300.87	95.27
44	6	62.97	808.29	3640.41	5358.35	64.88	53.61
51	7	46.44	710.89	2219.02	4809.94	51.39	95.67
58	8	49.32	577.48	1778.51	4393.19	57.67	51.44
65	9	78.80	739.84	1960.87	5278.68	73.09	73.60
70	10	65.24	467.11	1824.31	5096.81	52.96	207.20
79	11	45.69	508.16	1476.75	4403.78	47.12	47.94
85	12	48.48	450.23	2961.68	7458.88	46.83	46.92
91	13	73.06	624.03	2828.29	6407.97	160.41	48.30
97	14	49.41	635.78	1711.77	5075.03	48.93	95.82
114	15	50.20	486.40	2295.51	8611.68	48.35	64.19
121	16	38.37	392.63	2049.27	10884.99	53.99	48.94
132	17	63.24	561.69	5112.85	14751.03	60.45	66.00
147	18	218.57	507.92	4407.04	22238.80	83.45	69.85
149	19	33.00	516.23	4156.64	17726.36	60.44	36.24
156	20	29.37	900.48	3424.99	13830.84	46.32	40.67
163	21	26.65	468.60	2878.24	10819.43	26.67	32.51
169	22	25.53	303.69	3135.45	11372.83	29.11	29.78
176	23	61.50	3457.69	3753.87	8892.29	31.60	38.67
183	24	104.51	1767.55	3281.17	10372.47	21.62	21.44

[a] The detection limit of ICP-MS is 5 ppb. The uncertainty of ICP-MS is about 10%.

Information Only

Table B-2. pHr values of the starting brine solutions and the effluent of each reactor from 6-month SPFT experiments at 90 °C

Time, days	Week #	1.0 m NaCl	3.5 m NaCl	0.32 m $MgCl_2$	0.90 m $MgCl_2$	GWB	ERDA-6
0	0	8.6	8.6	7.9	7.4	7.4	8.3
8	1	8.2	8.0	8.2	8.9	6.8	7.5
17	2	8.5	8.3	8.0	7.9	6.8	7.8
23	3	8.4	8.3	8.4	8.2	6.9	7.9
30	4	8.0	7.9	8.1	7.9	7.0	8.1
37	5	8.0	8.0	8.1	7.9	6.8	8.0
44	6	8.0	8.0	8.1	7.9	6.9	8.1
51	7	8.2	8.2	8.2	7.9	7.1	8.1
58	8	8.5	8.6	8.2	7.9	7.0	8.0
65	9	8.3	8.5	8.1	7.8	7.0	8.1
70	10	8.4	8.6	8.0	7.8	7.1	8.1
79	11	8.4	8.4	7.8	7.6	7.1	8.2
85	12	8.4	8.5	8.1	8.1	7.1	8.2
91	13	8.7	8.9	8.2	7.8	7.1	8.3
97	14	8.8	9.0	8.2	7.9	7.1	8.3
114	15	8.5	8.4	8.2	8.1	7.1	8.3
121	16	8.6	8.3	7.9	8.0	7.1	8.3
132	17	8.6	8.3	7.9	8.0	7.2	8.3
147	18	8.6	8.3	7.9	8.0	7.1	8.1
149	19	8.6	8.3	7.9	7.9	7.1	8.2
156	20	8.3	8.2	7.7	8.0	7.2	8.2
163	21	8.3	8.3	7.9	8.1	7.0	8.1
169	22	8.3	8.3	8.2	8.2	7.1	8.3
176	23	8.2	8.3	8.2	8.2	7.1	8.2
183	24	8.2	8.3	8.2	8.3	7.1	8.2

Information Only